Towards alkali-stable polymers and hydroxide exchange membranes functionalized with alicyclic quaternary ammonium cations

Pham, Thanh Huong

2019

Document Version:
Publisher's PDF, also known as Version of record

Towards alkali-stable polymers and hydroxide exchange membranes functionalized with alicyclic quaternary ammonium cations

THANH HUONG PHAM | CENTRE FOR ANALYSIS AND SYNTHESIS | LUND UNIVERSITY

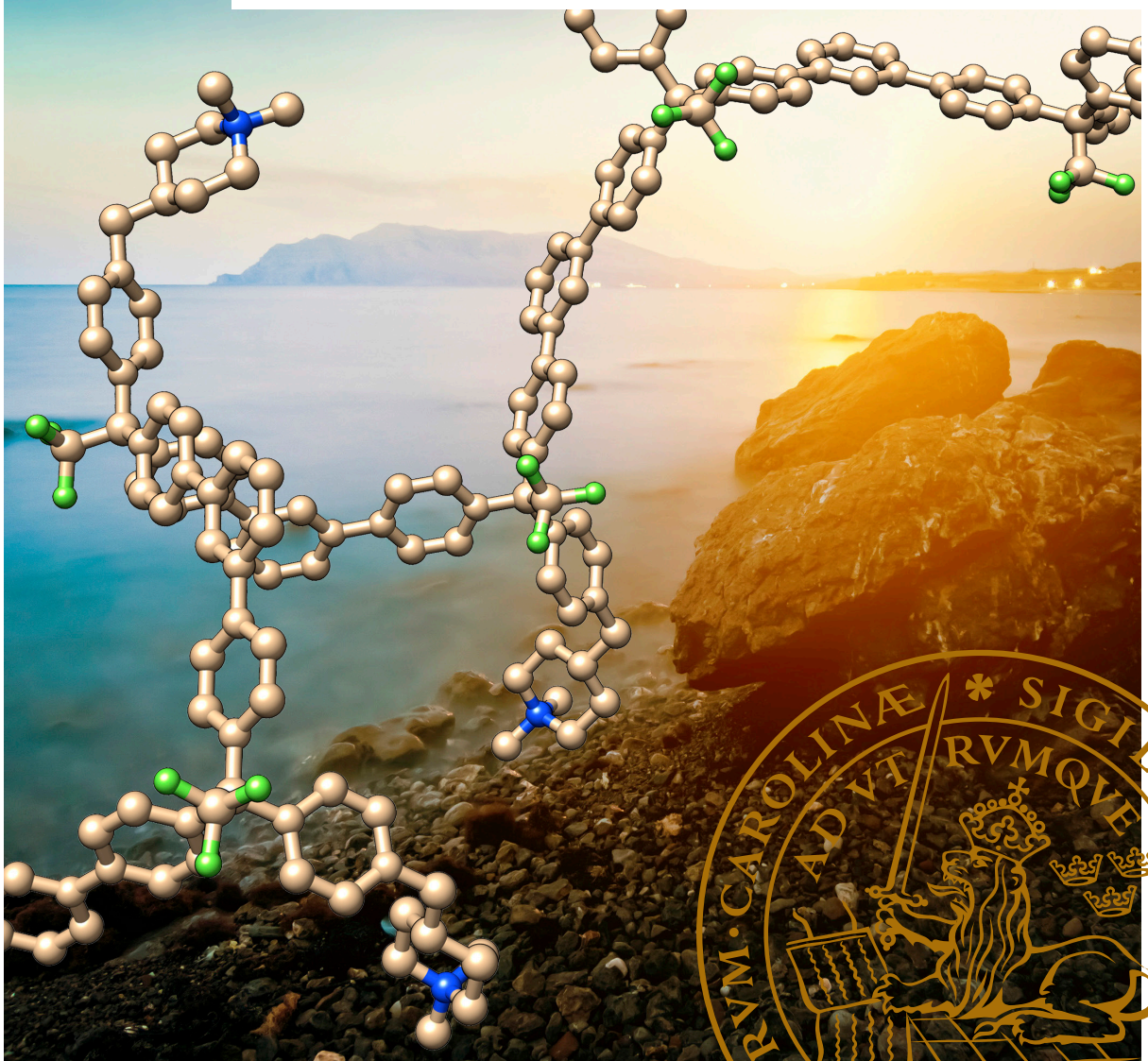

Towards alkali-stable polymers and hydroxide exchange membranes functionalized with alicyclic quaternary ammonium cations

Thanh Huong Pham

LUND
UNIVERSITY

DOCTORAL DISSERTATION
By due permission of the Faculty of Engineering, Lund University, Sweden.
To be defended at Kemicentrum, Lecture Hall K:B, on October 24, at 10.15

Faculty opponent
Dr. Jochen Meier-Haack, Leibnitz Institute of Polymer Research Dresden

Organization LUND UNIVERSITY	Document name Doctoral Dissertation
	Date of issue 2019-09-30
Author Thanh Huong Pham	Sponsoring organization

Title and subtitle

Towards alkali-stable polymers and hydroxide exchange membranes functionalized with alicyclic quaternary ammonium cations

Abstract

In the current work, cationic polymers functionalized with *N*-alicyclic quaternary ammonium (QA) cations were synthesized and characterized as potential hydroxide exchange membranes (HEMs) for application in fuel cells. Three different polymers, namely poly(arylene ether sulfone), spiro-ionene and poly(arylene alkylene), were explored as polymer backbones for the HEMs. Various mono- and spirocyclic QA cations were incorporated either within the backbone, directly on the backbone or via spacers. The synthesis of these polymers was a great challenge which was overcome with the help of numerous synthetic methods. Radical bromination, hydroboration and Suzuki coupling were employed when synthesizing the monomers. The backbone polymers were obtained by polyetherification, cyclo-polycondensation and super acid-mediated polyhydroxyalkylation. The mono- and spirocyclic QA cations were incorporated by quaternization and cycloquaternization, respectively.

The HEMs were characterized with regard to morphology, hydroxide conductivity, water uptake, thermal and thermochemical stability, i.e., the key properties that determine the performance and durability of the HEMs as electrolytes for hydroxide exchange membrane fuel cells. Studying the change in the properties as different chemical and structural features of the HEMs varied gave valuable insights into the structure-property relationships of theses materials, paving the way for further development of high performance HEMs for FC applications.

In this work, HEMs based on poly(arylene alkylene) functionalized with dimethylpiperidinium via spacers were found to possess the most attractive combination of properties. They had high hydroxide conductivities (103-146 mS cm^{-1}) and still maintained a reasonable water uptake (73-103%). Most importantly, they were exceptionally stable under alkaline conditions at elevated temperatures, with less than 5% ionic loss after 720 h of storage in 2 M NaOH solution at 90 °C.

Key words: hydroxide exchange membrane, fuel cell, alicyclic quaternary ammonium, alkali-stable, high hydroxide conductivity, structure-property relationship

Classification system and/or index terms (if any)

Supplementary bibliographical information		Language English
ISSN and key title		ISBN 978-91-7422-686-7 (Print) ISBN 978-91-7422-687-4 (Digital)
Recipient's notes	Number of pages 172	Price
	Security classification	

Signature _____ Date 2019-09-12

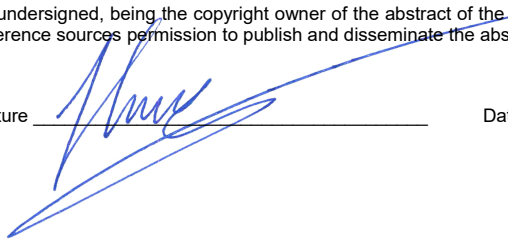

Towards alkali-stable polymers and hydroxide exchange membranes functionalized with alicyclic quaternary ammonium cations

Thanh Huong Pham

LUND
UNIVERSITY

Coverphoto front by Roman Gritcenko & 1xpert (Adobe Stock)
Coverphoto back by adimas (Adobe Stock)

Faculty of Engineering, Department of Chemistry
Centre for Analysis and Synthesis, Lund University

ISBN 978-91-7422-686-7 (Print)
ISBN 978-91-7422-687-4 (Digital)

Printed in Sweden by Media-Tryck, Lund University
Lund 2019

Media-Tryck is an environmentally certified and ISO 14001 certified provider of printed material. Read more about our environmental work at www.mediatryck.lu.se

List of Appended Papers

This thesis is based on the papers listed below

I. **Aromatic polymers incorporating bis-*N*-spirocyclic quaternary ammonium moieties for anion-exchange membranes**
Thanh Huong Pham and Patric Jannasch
ACS Macro Lett. **2015,** *4*, 1370-1375.

II. ***N*-spirocyclic quaternary ammonium ionenes for anion-exchange membranes**
Thanh Huong Pham, Joel S. Olsson and Patric Jannasch
J. Am. Chem. Soc. **2017**, *139*, 2888-2891.

III. **Poly(arylene piperidinium) hydroxide ion exchange membranes: synthesis, alkaline stability, and conductivity**
Joel S. Olsson, Thanh Huong Pham and Patric Jannasch
Adv. Funct. Mater. **2018,** *28*, 1702758.

IV. **Poly(arylene alkylene)s with pendant *N*-spirocyclic quaternary ammonium cations for anion exchange membranes**
Thanh Huong Pham, Joel S. Olsson and Patric Jannasch
J. Mater. Chem. A **2018,** *6*, 16537-16547.

V. **Effects of the *N*-alicyclic cation and backbone structures on the performance of poly(terphenyl)-based hydroxide exchange membranes**
Thanh Huong Pham, Joel S. Olsson and Patric Jannasch
J. Mater. Chem. A **2019**, *7*, 15895-15906

Papers not included in the thesis

VI. **Poly(*N,N*-diallylazacycloalkane)s for anion-exchange membranes functionalized with *N*-spirocyclic quaternary ammonium cations**
Joel S. Olsson, Thanh Huong Pham and Patric Jannasch
Macromolecules **2017,** *50*, 2784-2793.

VII. **Tuning poly(arylene piperidinium) anion-exchange membranes by copolymerization, partial quaternization and crosslinking**
Joel S. Olsson; Thanh Huong Pham and Patric Jannasch
J. Membr. Sci. **2019,** *578*, 183-195.

VIII. **Enzymatic synthesis and polymerization of isosorbide-based monomethacrylates for high-T_g plastics**
Livia Matt, Jaan Parve, Omar Parve, Tõnis Pehk, Thanh Huong Pham, Ilme Liblikas, Lauri Vares and Patric Jannasch
ACS Sustainable Chemistry & Engineering **2018,** *6*, 17382-17390.

IX. **Polyaromatic perfluorophenylsulfonic acids with high radical resistance and proton conductivity**
Narae Kang, Thanh Huong Pham and Patric Jannasch
ACS Macro Lett. **2019**, Accepted

X. **Ether-free polyfluorenes tethered with quinuclidinium cations as hydroxide exchange membranes**
Andrit Allushi, Thanh Huong Pham, Joel S. Olsson, Patric Jannasch
Submitted

My contributions to the publications

I. I planned and performed all the experimental work. I wrote the first draft of the paper

II. I planned and performed all the experimental work. I wrote the first draft of the paper

III. I took an active part in planning the project, analyzing/interpreting the results and writing the article.

IV. I planned and performed all the experimental work. I wrote the first draft of the paper

V. I planned and performed all the experimental work. I wrote the first draft of the paper

Abbreviations

AEM	anion exchange membrane
AFC	alkaline fuel cell
aq.	aqueous
ASU	6-azaspiro[5.5]undecan-6-ium
DCM	dichloromethane
DIPEA	*N,N*-diisopropylethylamine
DMP	dimethylpiperidinium
DMSO	dimethylsulfoxide
E2	bimolecular elimination
FC	fuel cell
HEM	hydroxide exchange membrane
IEC	ion exchange capacity
NMP	*N*-methyl-2-pyrrolidone
PAA	poly(arylene alkylene)
PAES	poly(arylene ether sulfone)
PEM	proton exchange membrane
QA	quaternary ammonium
S_N2	bimolecular substitution
TFA	trifluoroacetic acid
TFAc	1,1,1-trifluoroacetone
TFSA	trifluoromethanesulfonic acid
TMA	trimethylammonium
TPAp	2,2,2-trifluoroacetophenone

Table of Contents

1. Introduction 1
1.1. Hydroxide exchange membranes for fuel cells 1
1.1.1. The fuel cell 1
1.1.2. Hydroxide exchange membranes-requirements and challenges 5
1.2. Strategies to improve alkaline stability 9
1.2.1. The cationic groups 9
1.2.2. The backbone polymers 12
1.3. Overview of the thesis work 13
2. Experimental methods 16
2.1. Polymer synthesis and characterization 16
2.1.1. Backbone polymers 16
2.1.2. Incorporation of alicyclic quaternary ammonium cations 20
2.1.3. Characterization 23
2.2. Membrane preparation and characterization 25
2.2.1. Membrane preparation and morphology 25
2.2.2. Water uptake and hydroxide conductivity 27
2.2.3. Thermal and alkaline stability 29
3. Summary of appended papers 31
3.1. Hydroxide exchange membranes based on poly(arylene ether sulfone)s (Paper I) 31
3.2. Spiro-ionenes (Paper II) 34
3.3. Hydroxide exchange membranes based on poly(arylene alkylene)s (Paper III-V) 37
3.3.1. Effect of cations (Paper III-IV) 38
3.3.2. Effect of spacer and backbone structure (Paper V) 43
3.4. Influence of chemical structure on the alkaline stability of hydroxide exchange membranes 46
4. Conclusion and future outlook 49

5. Popular science summary.....51
6. References.....53
7. Acknowledgements.....61

1. Introduction

1.1. Hydroxide exchange membranes for fuel cells

Global warming, caused by too high levels of atmospheric carbon dioxide, is currently one of the most serious issues the world is facing. In order to reduce the emission of carbon dioxide, extensive efforts have in the last decades been invested in developing methods to replace fossil fuels with more sustainable and environmentally friendly energy sources, including wind power, solar power and biofuels.[1-3] Many electrochemical devices, such as redox flow batteries,[4-9] water electrolyzers[10-15] and fuel cells (FCs)[4, 16-19] are required to efficiently use these intermittent energy sources by converting and storing the energy produced. Ion exchange membranes (IEMs) are currently widely employed as separators in these devices.[14, 20-23] As key components, they will directly or indirectly affect the performance and life-time of these devices. Hence, the IEMs must be tailored to satisfy the specific requirements set by the application.

IEMs are semipermeable membranes that conduct specific ions but prevent the cross-over of gases.[24] IEMs can be classified based on the nature of the ions conducted into two main types: anion exchange membranes (AEMs) and cation exchange membranes. As the names imply, AEMs facilitate the transport of anions while cation exchange membranes facilitate the transport of cations.[24] In this thesis work, AEMs in the specific hydroxide form are referred to as hydroxide exchange membranes (HEMs) and cation exchange membranes in the proton form are denoted proton exchange membranes (PEMs).

The focus of this thesis work has mainly been directed toward the development of HEMs for application in FCs. Therefore, this section gives a brief introduction of these devices and their requirements on the HEMs applied.

1.1.1. The fuel cell

History

The first FC prototype was studied as early as 1839 and was named “gas voltaic battery” by its inventor, Sir William Robert Grove.[25-26] This early prototype

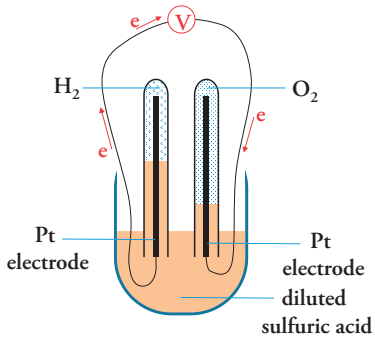

Figure 1. Schematic representation of a cell in Grove's gas voltaic battery

consisted of two platinum electrodes and diluted sulfuric acid electrolyte. The electrodes were immersed in the electrolyte at one end and separately sealed in glass tubes containing oxygen and hydrogen at the other end (**Figure 1**). With this arrangement, Grove discovered that he could generate a constant electrical current between the electrodes and the liquid rose in both glass tubes. The electrical current generated by Grove's fuel cell was low and thus did not have much practical significance at the time.

A major advance in fuel cell technology development came much later, around the mid-1900s. In August 1959, Francis Thomas Bacon demonstrated the first useful fuel cell system that consisted of 40 cells and could reach up to 5 kW.[27] Bacon's cell was the earliest version of an alkaline fuel cell (AFC), a FC that has an alkaline as opposed to an acidic electrolyte. An improved version of the AFC was later employed to power the Apollo space vehicle.[28] The space programme in the late 1950s and early 1960s played an important role in the development of fuel cells. The proton exchange membrane fuel cell (PEMFC) was also born during this period. An early version of the PEMFC, invented by Willard Thomas Grubb and refined by Leonard Niedrach, was used in the Gemini space program in the mid-1960s.[29]

In recent years, fuel cells have received renewed interest due to their potential as environmentally friendly alternatives to for instance internal combustion engines (ICEs). In an ICE, the fuel is directly oxidized by oxygen in a combustion chamber to generate thermal energy, which is further transformed into useful mechanical energy.[30] Under ideal conditions, the thermal efficiency of ICEs is limited by the Carnot cycle, but in reality, the efficiency of ICEs is even lower due to factors such as incomplete combustion, energy loss as heat, friction, etc.[30] The efficiency of a typical gasoline combustion engine used in a car is about 20%.[31-32] Meanwhile, FCs continuously convert chemical energy stored in fuels directly into usable electrical energy at a high efficiency up to 65%. FC systems that co-generate electricity and heat can reach even higher overall efficiencies, up to 90%.[33] Furthermore, FCs have a high potential to utilize renewable energy sources such as hydrogen, methanol and

ammonia instead of the fossil fuel. The use of FCs also reduces the release of pollutants such as CO, NO_x and hydrocarbons formed as by-products in ICEs.[34]

Fuel cell types

FCs can be classified based on the type of electrolyte used. Several types of FCs are listed below:

- AFC: The electrolyte is a liquid alkaline solution. AFC is one of the earliest developed FC systems.[35-36]
- PEMFC: The electrolyte is a PEM. Currently, the most commonly used PEM in PEMFCs is Nafion®, a sulfonated perfluorinated polymer (**Figure 2**). PEMFCs are already commercialized as a power source for various vehicles, mobile devices and military equipment.[18, 37-43]

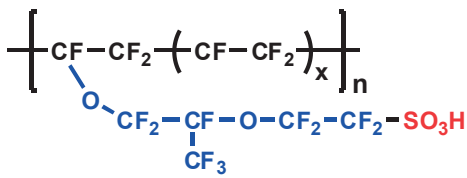

Figure 2. Chemical structure of Nafion®

- HEMFC: The electrolyte is a HEM. The development of alkali-stable HEMs for application in FCs is the focus of this thesis work. This type of FC is also called alkaline anion exchange membrane fuel cell (AAEMFC) or just anion exchange membrane fuel cell (AEMFC) in the literature.[35]
- Solid acid fuel cell: The electrolyte is an inorganic solid acid material, e.g. $CsHSO_4$ or CsH_2PO_4.[44-45]
- Phosphoric acid fuel cell (PAFC): The electrolyte is phosphoric acid. PAFC usually operates at ~150 – 200 °C.[46]
- Solid oxide fuel cell (SOFC): The electrolyte is a solid non-porous ceramic that can conduct oxide ions (O^{2-}). SOFCs operate at very high temperatures (800 - 1000 °C). [47-48]

Working principles

When Grove first introduced his "gas voltaic battery", the first FC prototype in the 1800s, it stirred up a debate within the scientific community over how it worked. Thankfully, the working principles of an FC is no longer a mystery for the scientist nowadays. FCs generate electricity by splitting the redox reaction between fuel and oxygen into two separated half reactions at the anode and cathode.[36] As an example, the conversions of hydrogen under acidic and alkaline condition in a PEMFC and HEMFC are shown in **Figure 3a** and **b**, respectively.[35] A catalyst is necessary to lower

the activation energy and enable the reactions at both the cathode and anode. Thanks to the electrolyte that separates the two electrodes and allows only one type of ion to be transported through it, a potential is built up between the electrodes. The theoretical open circuit potential is low and depends on the fuel type. When H_2 is employed, the maximum cell potential is ~1.23 V. This value is ~1.18 V for methanol. The actual voltage is in reality even lower and will drop with increasing current density. In order to reach sufficient output voltage, the FCs are assembled in series in an FC stack.[36]

Advantages and disadvantages of PEMFCs, AFCs and HEMFCs

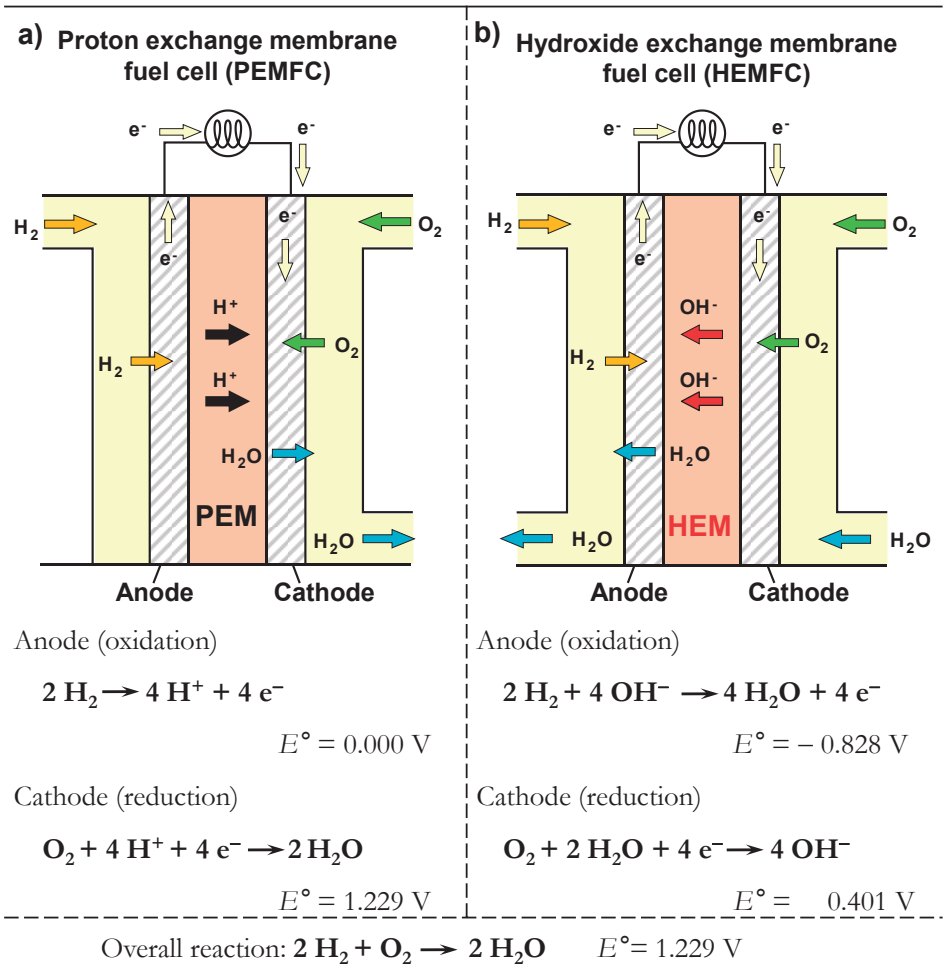

Figure 3. Schematic illustration of a PEMFC (a) and an HEMFC (b) and the reactions taking place when hydrogen gas is used as a fuel.

As can be seen in **Figure 3**, provided that the fuel type is the same, the overall reaction and cell potential are identical for both types of fuel cells. However, the specific half reactions and their reaction potentials differ due to the dissimilarity in pH. The necessity of using the scarce and expensive Pt catalyst for the reactions under acidic condition severely limits the availability and increases the cost of production of PEMFCs, thereby impeding the wide commercialization of this type of FC. In comparison, FCs operating under alkaline conditions have the advantage of a more facilitated oxygen reduction reaction (ORR) which enables a wider choice of catalyst, e.g., Ag, Co, Fe and diverse inorganic oxides.[49-59]

An AFC comprising a liquid alkaline solution as the electrolyte was the first fuel cell system operating under alkaline conditions. In comparison with PEMFCs, AFCs have some disadvantages. The first and most important disadvantage is that the liquid alkaline electrolyte readily absorbs CO_2 (from the air supply) to form carbonates:[60]

$$2OH^- + CO_2 \rightarrow CO_3^{2-} + H_2O$$

$$OH^- + CO_2 \rightarrow HCO_3^-$$

This consumes hydroxide ions and consequently decreases the cell current. More seriously, it also leads to carbonate precipitate, which can block the electrodes and prevent gas diffusion. Another disadvantage of the AFCs is the higher risk of leakage of the very corrosive liquid electrolyte in comparison with the solid polymeric electrolyte in PEMFC.[35]

Therefore, an HEMFC that combines the advantages of alkaline operating conditions with a solid polymeric electrolyte seems to be an ideal system. However, the HEMFC technology is currently not as well-developed as PEMFC. One of the main issues hindering the development of HEMFCs is the lack of a high-performing HEMs suitable for application in FCs. In the next section, the specific requirements for HEMs in FCs and the main challenges of their development is discussed.

1.1.2. Hydroxide exchange membranes-requirements and challenges

Requirements

As already mentioned above, to be used as an electrolyte in FCs, the HEM must maintain an efficient transport of hydroxide ions from the cathode to the anode, but at the same time still ensure the separation of the electrodes. Therefore the HEM must fulfill the following requirements:[52, 61-63]

- High hydroxide conductivity
- High mechanical, thermal and chemical stability

- Low fuel and gas permeability

Furthermore, for practical use, HEMs should be able to be readily produced on a large scale and at low cost.

Challenges

In the infancy of the field, the low hydroxide conductivity and the low thermochemical stability were considered the two main challenges for the development of HEMs for FCs.[35, 52] HEMs generally have a lower conductivity in comparison with PEMs with similar ion exchange capacity (IEC) due to two reasons:

- Hydroxide ions have a lower mobility than protons. In a dilute solution at 25 °C, the mobility of hydroxide ions is approximately 1.8 times lower than that of protons.[64]
- HEMs and PEMs typically consist of hydrophobic polymeric backbones tethered with ionic groups. The cationic groups of HEMs generally have a lower level of dissociation than the anionic groups of PEMs.

However, the concern about the low level of dissociation of hydroxide ions might be overstated. At high water contents, the transport coefficients of hydroxide ions in HEMs approach those in pure water, suggesting complete dissociation.[65] The difference in degree of ionic dissociation between HEM and PEM is however more prominent at low water contents.[66-67] The reason for this behavior is the less developed phase-separated nano-morphology in HEMs. The formation of hydrophilic/ hydrophobic phase separation in a HEM is much more challenging than in for instance Nafion, because the hydrophobicity of the hydrocarbon polymer backbone of HEMs is generally lower than that of the fluorocarbon backbone of Nafion.[39] In addition, in HEMs, the cations are often connected to the polymer backbone via short side chains which do not assist in the ion cluster formation as effectively as the rather flexible side chains in Nafion.[68-72]

The most straightforward solution for the low conductivity problem is to increase the IEC of the HEMs. This has two positive effects on the hydroxide conductivities since an increase in IEC will increase not only the concentration of cations, but also the uptake of water, which is necessary for the formation of the conducting percolating water-rich channel system. However, this strategy must be adopted with care, because extensive water uptake causes dilution of cations and consequently decreases the conductivity.[73] Furthermore, a too high water uptake will lead to a high degree of swelling and deterioration of the mechanical properties.[73-74] Another plausible method to enhance the hydroxide conductivity without sacrificing the mechanical integrity is by promoting phase separation by extending the links between the cations and polymer backbones. This is however a significant challenge for polymer synthesis, which calls for new synthetic methods. By combining both

methods, many research groups have succeeded in producing HEMs with conductivities exceeding 100 mS cm^{-1} at 80 °C, which is needed for a high FC current density.[63, 75-86]

The other major challenge, i.e., the low thermochemical stability of HEMs in the working conditions at high pH, might be more difficult to overcome. The highly nucleophilic hydroxide ions readily attack both the cations and the polymer backbone of HEMs. Depending on the chemical structure of the cations, they can degrade via a number of different degradation pathways. For example, quaternary ammonium (QA) cations can degrade via Hofmann elimination,[87-89] nucleophilic substitution,[90-91] Sommlet Hauser rearrangement and Stevens rearrangement

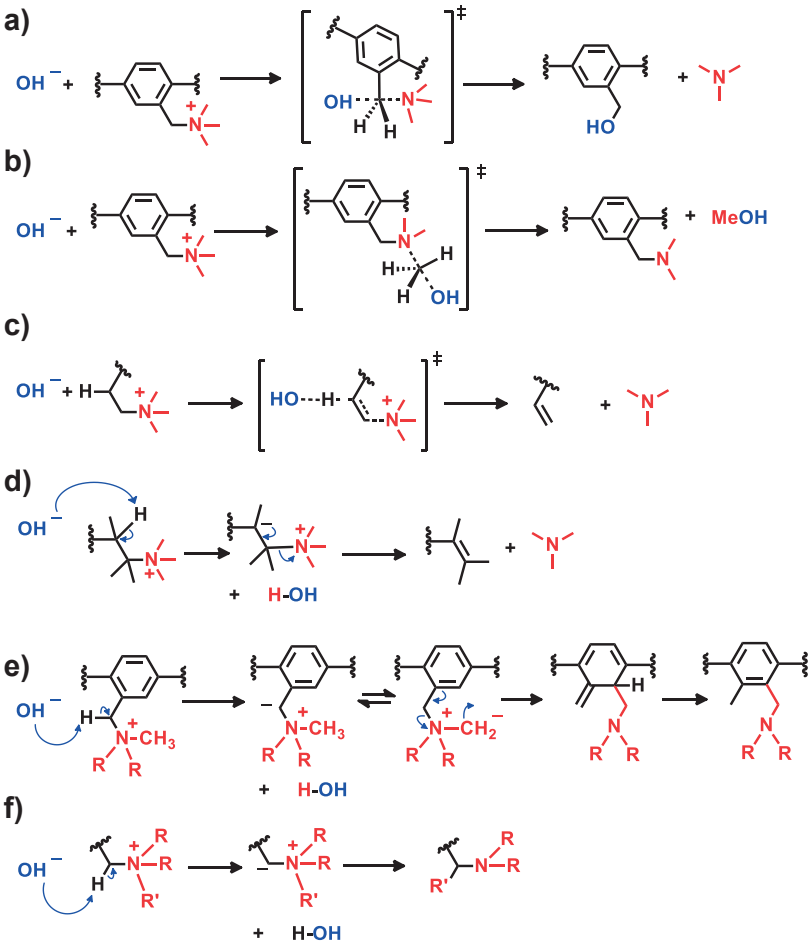

Scheme 1. Some degradation pathways of QA cations, including nucleophilic substitution at benzyl (a) and methyl (b) positions, Hofmann elimination (E2) (c), E1cb elimination (d), Sommlet Hauser rearrangement (e) and Stevens rearrangement (f).

(**Scheme 1**).[92-94] Regarding the polymer backbone, the cleavage of the aryl ether bond is the main degradation mechanism for many polymers including poly(arylene ether sulfones) (PAES) and poly(*p*-phenylene oxide) (PPO) (**Figure 4a** and **Figure 4b**).[95-100] Consequently, polymers free from aryl-ether linkages, such as poly (arylene alkylene)s (PAAs), polyphenylenes and fluorene-based polymers (**Figure 4c-f**) are more suitable backbones for HEMs. [78-79, 101-105]

In addition, the combination of alkali-stable cations with an alkali-stable backbone does not necessarily result in an alkali-stable HEM.[99, 106-107] Therefore, the alkaline stability of the cations and backbone cannot be treated separately but must always be evaluated together. In the search of alkali-stable HEMs, various strategies have been used, including but not limited to employment of β-hydrogen-free cations and an ether-free backbone, utilization of steric protection,[108-110] conformational restriction,[75, 81, 91, 111-113] resonance and inductive effects.[78, 114-120] These strategies are discussed in more detail in the following section.

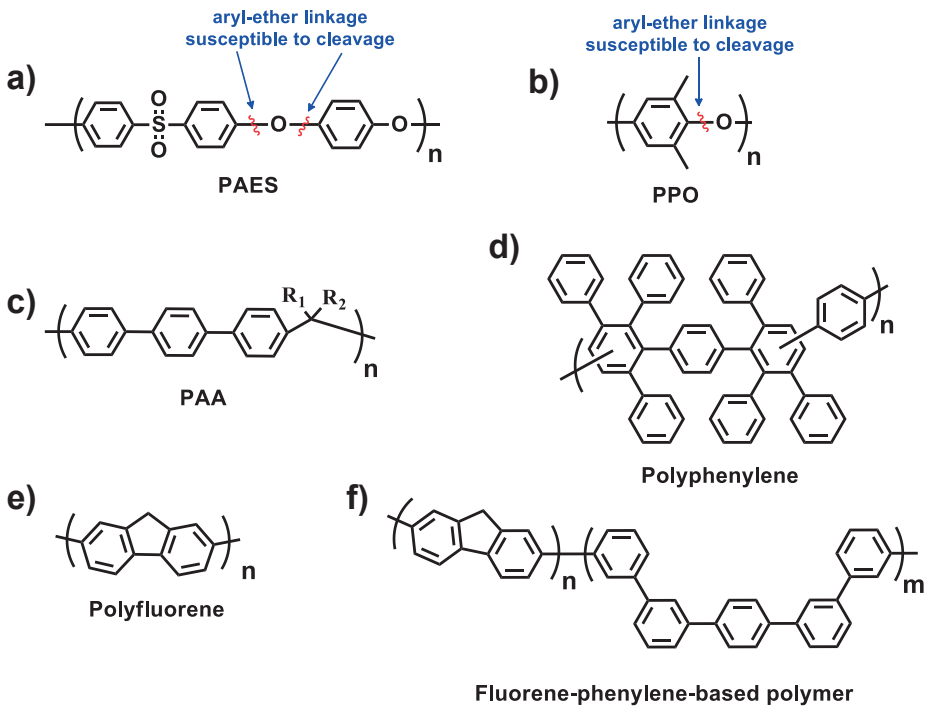

Figure 4. Some examples of polymer backbone for HEMs, including a PAES (a), a PPO (b), a PAA (c), a polyphenylene (d), a polyfluorene (e) and a fluorene-phenylene-based polymer (f).

1.2. Strategies to improve alkaline stability

1.2.1. The cationic groups

Quaternary ammonium cations

Table 1.Half-lives of some QA cations in 6 M NaOH at 160 °C

QA cation	Abbreviation	Half-life [h]
	TMA	61.9
	ETM	2.8
	PTM	33.2
	NTM	20.7
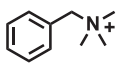	BTM	4.18
	DMPy	37.1
	DMP	87.3
	ASD	28.4
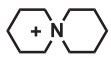	ASU	110

QA cations are the most frequently used and extensively studied cations for HEMs due to their synthetic accessibility and inexpensive starting materials. The Hofmann elimination (**Scheme 1c** and **d**) has generally been considered the main degradation mechanism for most QA cations.[52, 91] Consequently, a common strategy to achieve alkali-stable HEMs is to employ QA cations that lack β-hydrogens and cannot degrade via this pathway. However, in the absence of Hofmann elimination, other degradation mechanisms usually become prominent. For example, benzyltrimethylammonium (BTM) degrades readily via nucleophilic substitution at the benzylic position to form benzyl alcohol and trimethylamine (**Scheme 1a**). Similarly, neopentyltrimethylammonium (NTM), which contains no β-hydrogens, decomposes even more rapidly than propyltrimethylammonium (PTM), which

contains two β-hydrogens (**Table 1**). The mechanism of degradation of NTM is complex, with major degradation products arising from S_N2 attack/ylide formation but other minor unidentified degradation products have also been detected.[87, 91]

Despite the concern about more facile Hofmann elimination, the introduction of longer alkyl spacers between QA cations and the polymer backbone can actually improve the alkaline stability of both QA cations and the polymer backbone. A study on small model compounds by Marino and Kreuer revealed that, while ethyltrimethylammonium (ETM) cations are unstable under alkaline conditions, the alkaline stability improved significantly when the length of the alkyl chain was extended to 3 or 6 carbon atoms.[91] This behavior might be a result of both the induction effect and steric shielding by the long alkyl chain. However, the stability dropped again when the alkyl chain was further extended to contain 8 carbon atoms or more (**Figure 5**), suggesting that the mechanism is more complex.[91] Nevertheless, a number of recent studies have proven that implementing long alkyl spacers is a viable strategy to design and prepare alkali-stable HEMs. [77-79, 101-102, 111, 114, 121-122]

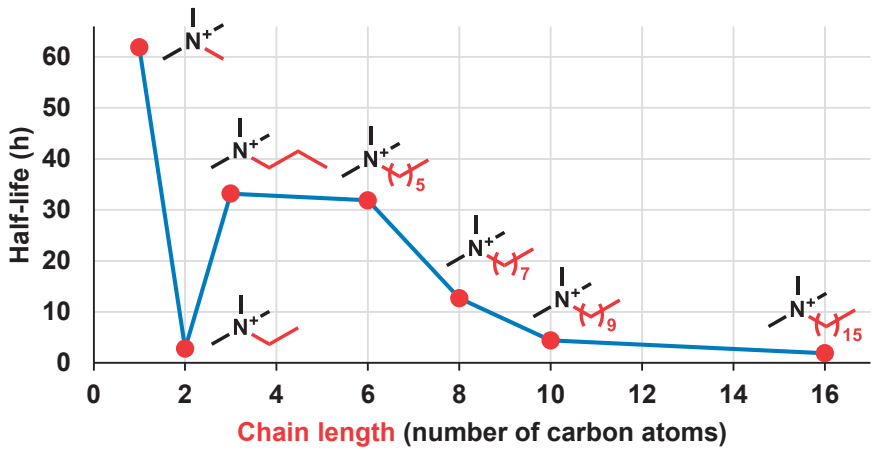

Figure 5. Half-life of different trimethylalkylammonium cations in 6M aq. NaOH solution at 160 °C as a function of the alkyl chain-length.[91]

Introducing substitution groups at α and β positions is another approach to alkali-stable QA cations. The increased steric hindrance at these positions can prevent the nucleophilic attack of hydroxide ions, therefore reducing Hofmann elimination via the E2 mechanism (**Scheme 1c**). However, the presence of quaternary and tertiary carbons may enable other degradation mechanisms, e.g., E1cb elimination (**Scheme 1d**).[90]

A strategy that has proven effective in reducing the degradation of QA cations in alkaline conditions is conformational restriction. The two major degradation pathways via E2 and the S_N2-mechanism proceed via the formation of transition

state complexes with specific bond angles (**Scheme 1a-c**). Consequently, the formation of the transition state complexes for alicyclic QA cations, such as dimethylpiperidinium (DMP), dimethylpyrrolidinium (DMPy), 5-azaspiro[4.5]decan-5-ium (ASD) and 6-azaspiro[5.5]undecan-6-ium (ASU), requires a significant deformation of the stable 5- and 6-membered rings, leading to an increase in activation energy and stability. The remarkable alkaline-stability of the alicyclic QA cations mentioned above was reported in a seminal work by Kreuer and Marino.[91] Amongst the 26 QA cations investigated in the study, ASU and DMP had the longest half-lives of 110 and 87.3 h, respectively, in 6 M aq. NaOH at 160 °C. Under the same conditions, DMPy and ASD, showed half-lives of 37.1 and 28.4 h, respectively and were less stable than TMA (61.9 h) but still more stable than BTM (4.18 h) (**Table 1**).

The most straightforward pathway to incorporate alicyclic QA cations into HEMs is via Menshutkin reactions of methylpiperidine or methylpyrrolidine with a benzyl or alkyl halide. The alicyclic QA cations are then connected to the polymer backbone via substitution at the 1,*N*-position (**Scheme 2**). Even though an improvement in alkaline stability was observed,[75] the hydroxide ions can still attack the labile benzyl carbon or the anti-periplanar β-hydrogens in the alkyl chain. A more ideal approach to utilize the conformational restriction of the alicyclic QA cations is to attach them to the polymer via the 3- or 4- position instead. This is, however, quite a challenge from a synthetic point of view.

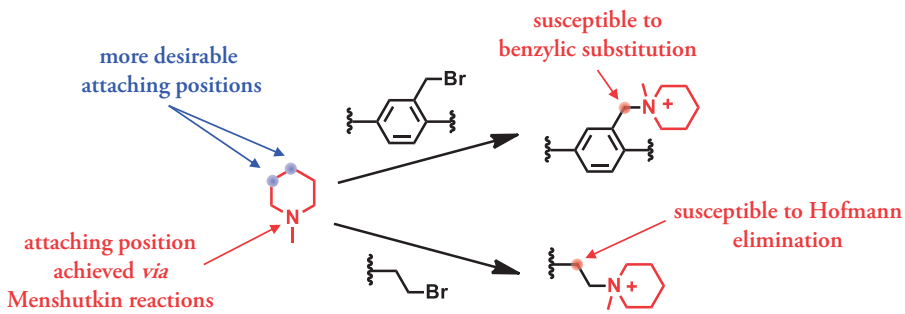

Scheme 2. Menshutkin reactions of *N*-methylpiperidine with benzyl or alkyl bromide, respectively.

Imidazolium

In addition to QA cations, different *N*-based cations have also been actively investigated as potential cationic groups for HEMs. Amongst these, imidazolium and benzimidazolium-based cations are the most promising candidates. Imidazolium cations without substituents at the C2-positions (**Scheme 3**, R_2=H) are unstable

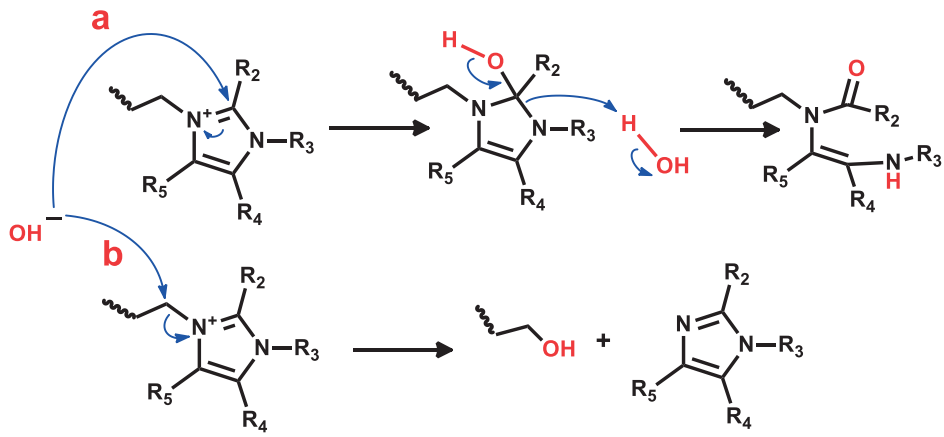

Scheme 3. Degradation of imidazolium cations via ring-opening (a) and dealkylation (b).

under alkaline conditions and can decompose via ring-opening (**Scheme 3a**) or dealkylation (**Scheme 3b**). The introduction of bulky substituents at the C2-position sterically protects the cations against nucleophilic attack at this position, thus preventing ring-opening degradation. Long alkyl chain substituents at the N1- and N3-positions have been reported to suppress dealkylation. A number of poly(benzimidazoliums) and poly(arylimidazoliums) with high alkali stabilities have recently been reported to give promising results in fuel cell testing.[123-126]

1.2.2. The backbone polymers

The polymer backbones are not only responsible for the structural integrity and mechanical strength, but also have a substantial impact on the chemical stability of HEMs. The chemical degradation of the backbone is a significant issue as it can lead to cleavage of polymer chains and a decrease in the molecular weight of the polymer. This might eventually result in membrane breakage and collapse/failure of the device. Various polymers, including PAES, PPO, polyphenylene and PAAs, have been employed as backbone for HEMs (**Figure 4**). Recently, Bae and Mohanty et al. performed a systematic study to investigate and compare the alkaline stability of nine representative polymer structures. Among these, PAESs were found to have the lowest alkaline stability, followed by PPOs. The main degradation pathway for these polymers was aryl ether bond cleavage.[96] While both non-functionalized PAES and PPO are quite stable at high pH,[127] the presence of the strong electron-withdrawing cationic groups in close proximity to the aryl ether bond significantly accelerated its cleavage. Thus, one strategy to improve the alkaline stability for the polymer backbones would be to attache the cations via long alkyl chains instead of the short methylene link as in the widely used benzyltrimethylammonium cation. Another

strategy is to employ aryl ether-free polymers, such as poly(phenylene)s and PAAs instead. Both strategies have been successfully employed to prepare alkali-stable HEMs.

1.3. Overview of the thesis work

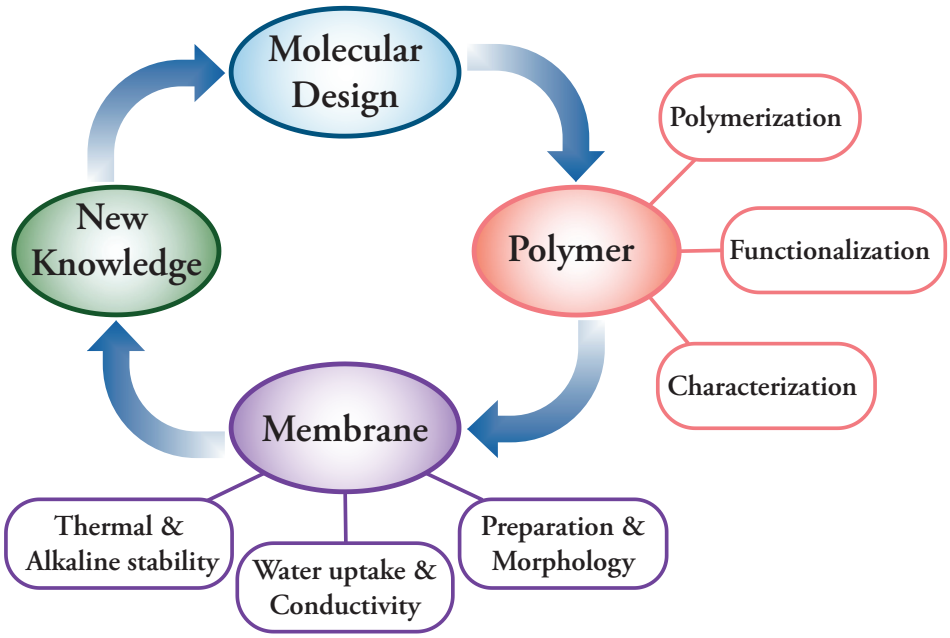

Figure 6. Research methodology to develop HEMs for fuel cells.

The main goal of this thesis work is to synthesize alkali-stable polymers and HEMs suitable for application in HEMFCs. Based on previous knowledge acquired from the literature and own research, each project in this thesis started with the molecular design of the cationic polymers. The designed polymers were synthesized and HEMs were prepared and characterized with regard to their morphology, water uptake, hydroxide conductivity, thermal stability and alkaline stability. The results provided new knowledge about the structure-property relationships of the HEMs and contributed to further development (**Figure 6**).The alkaline stability of the HEMs was the main focus and the first consideration in the molecular design, followed by hydroxide conductivity and water uptake.

Inspired by the promising results reported by Marino and Kreuer regarding the highly alkali-stable alicyclic QA cations, these cations were selected as cations for

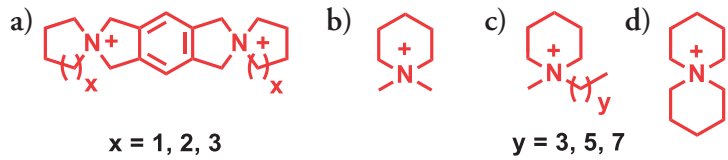

Figure 7. The alicyclic QA cations employed as cations for HEMs in this thesis work.

HEMs throughout this thesis work (**Figure 7**). The influence of the structure of the cations on the stability of HEMs was also investigated.

In comparison, the choice of polymer backbones is usually less straightforward as each polymer type has its own advantages and disadvantages. Therefore, throughout this work, different polymers, namely PAES, spiro-ionene and PAA (**Figure 8**) were utilized as the polymer backbone and their influence on the properties of the resulting membranes was explored.

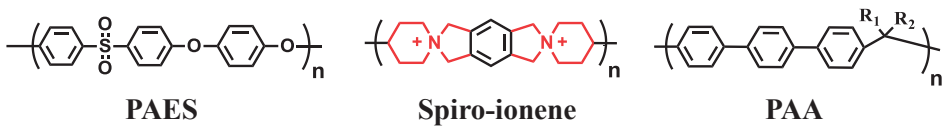

Figure 8. Representative structures of the polymer backbones studied in this thesis work.

Another factor that can affect the alkaline stability of the HEMs is the placement of the cations along the polymer backbone. Here, three different polymer architectures were explored as shown in **Figure 9**. Representative chemical structures of the resulting polymers are summarized in **Figure 10**.

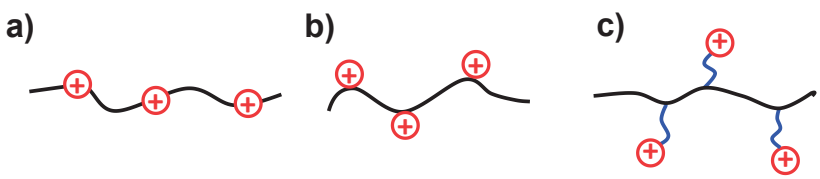

Figure 9. Schematic illustration showing the three polymer architectures employed. The cations were incorporated in the polymer backbone (a), attached directly on the polymer backbone (b) or connected to the backbone via spacers (c).

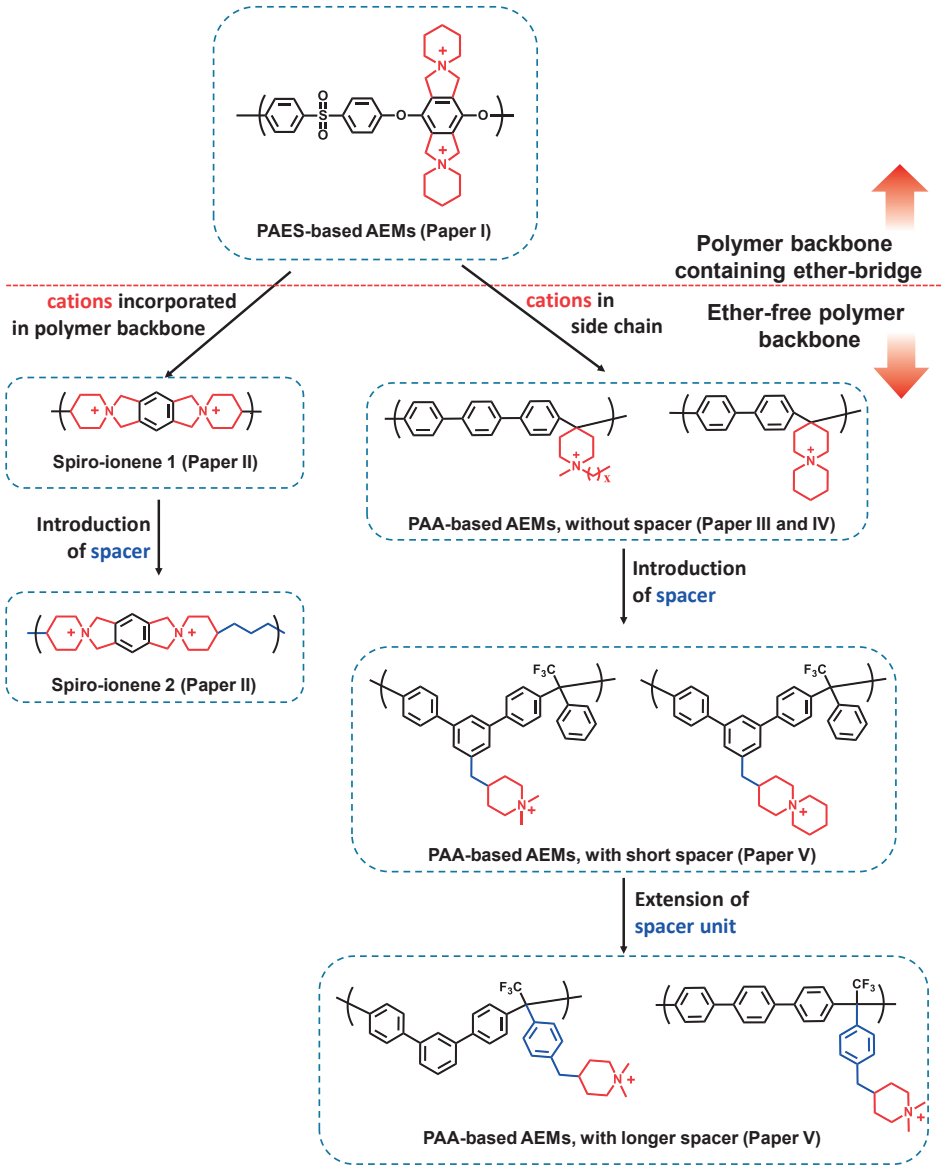

Figure 10. Representative structures of the cationic polymers synthesized in this thesis work.

2. Experimental methods

This chapter introduces the main experimental methods employed throughout the thesis. It is divided into two parts with different focus. The focus of the first part is on the cationic polymer; the various strategies employed to synthesize the polymers and the methods used to characterize them. The second part will cover the general methods for fabricating and characterizing the HEMs based on these polymers.

2.1. Polymer synthesis and characterization

2.1.1. Backbone polymers

Poly(arylene ether sulfone)s

PAESs possess superior properties such as high thermal and hydrolytic stabilities, an elevated chemical resistance, decent electrical and mechanical properties, as well as flame retardancy. Thus, they are widely used as high-performance polymers in biomedical, electrical, food-processing and other applications that require a high-temperature tolerance.[128-131] Sulfonated PAESs have been employed as PEMs in both hydrogen/air and direct methanol fuel cells instead of the bench-mark Nafion. Many PAES membranes have displayed similar or even better performance than Nafion.[131-133] Commercial PAESs were developed as early as in the 1960s independently by the 3M Corporation, the Union Carbide Corporation, and the plastics division of ICI.[134]

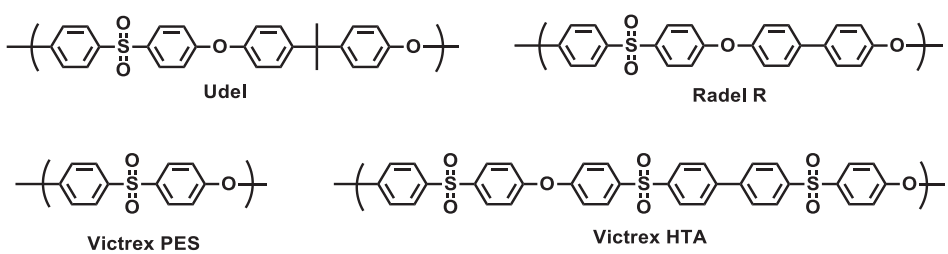

Figure 11. Some examples of commercial PAESs.

Nowadays, a wide variety of PAESs are commercially available under different trademarks; e.g. Udel, Radel, Victrex, Astrel (**Figure 11**).[135]

There are two main synthetic routes to PAESs: polysulfonylation and polyetherification.[136] In polysulfonylation, the sulfonyl linkages are formed in Friedel-Crafts type reactions of aryl sulfonyl chlorides and aromatic substrates (**Scheme 4**). The aryl sulfonyl chlorides first form aryl sulfonyl cations, which subsequently carry out electrophilic attacks on the aromatic substrates. Since the attacks can happen at both *o*- and *p*-positions, the PAESs synthesized by this route have a less defined structure and can be branched (**Scheme 4**).

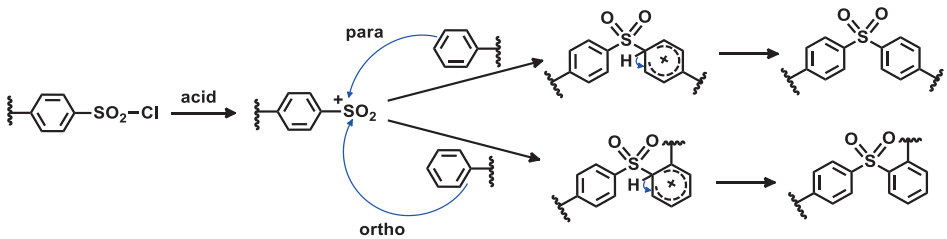

Scheme 4. Synthesis of PAESs via polysulfonylation.

The second route, polyetherification, can proceed without this complication and was chosen as the method for synthesizing PAES backbones in the present work. A polyetherification is a typical nucleophilic aromatic substitution (S_NAr) reaction, where the halogens in activated aryl chlorides or aryl fluorides are displaced by phenolate anions (**Scheme 5**). The aryl fluorides are generally more reactive than aryl chlorides, but are also more expensive. Therefore, 4,4'-dichlorodiphenyl sulfone was the reactant of choice for the PAES synthesis herein. The phenolate anions were produced *in situ* by addition of K_2CO_3 together with the diphenols bisphenol A and tetramethylhydroquinone.

The solvent is another important parameter that strongly influences the efficiency of the polymerization. The solvent for polyetherification must be able to dissolve both the reactants and the growing polymer chain without leading to side reactions. Hence, polar aprotic solvents such as dimethylsulfoxide (DMSO), *N,N*-dimethylformamide, *N,N*-dimethylacetamide (DMAc) or *N*-methyl-2-pyrrolidone

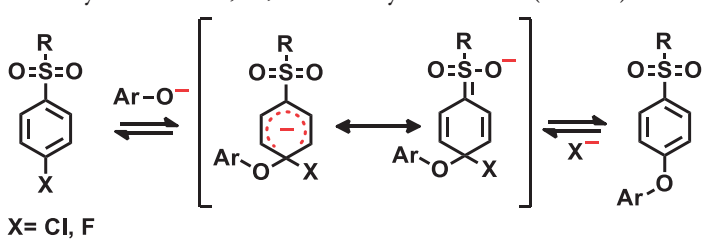

Scheme 5. Reaction mechanism of polyetherification (S_NAr).

(NMP) are most suitable. The solvent must be polar in order to solvate the phenolate ions and aprotic to avoid the solvolysis of the phenolate.[137] The presence of water is undesirable because water limits the conversion and consequently the molecular weight of the PAES. Water was therefore removed by azeotropic distillation of the reaction mixture using toluene. In order to enhance the solubility of the phenolate and the reaction rate of the polymerization, the temperature of the reaction was kept high. The temperature is however limited by the thermal stability of the reactants and the boiling point of the solvent.

Spiro-ionenes

The spiro-ionene backbones are quite unique as the cations are directly incorporated in the backbone. The synthesis of a spiro-ionene with unique rod-like structure (**Figure 12**) was reported by Müllen et al. in 1990.[138] The polymers are formed by cyclo-polycondensation between diamines and 1,2,4,5-tetrakis(bromomethyl) benzene. The cyclo-polycondensation reaction is in fact a series of consecutively repeated cycloquaternization reactions, which will be further discussed in **Section 2.1.2**.

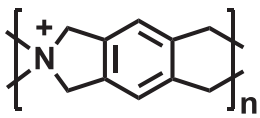

Figure 12. An ionene with a spirane structure.[138]

Poly(arylene alkylene)s

The ether-free PAA backbones were synthesized by Friedel-Crafts type polyhydroxyalkylations. The Friedel-Crafts hydroxyalkylation reactions are widely used in the synthesis of organic compounds. For example, bisphenol A is synthesized by a Friedel-Crafts hydroxyalkylation between acetone and phenol.[139] In a typical Friedel-Crafts hydroxyalkylation, an electron-rich arene, activated by electron-donating groups, is condensed with a ketone or aldehyde in an acidic medium. By employing a super acidic medium, even non-activated arenes can be used in reactions with electron-poor aldehydes or ketones. The reaction is highly efficient and can be used to synthesize polymers with high molecular weight. Recently, it has been recognized as one of the few routes to ether-free polymer backbones.[9, 79, 103, 140-143] In this thesis, various PAAs were successfully synthesized by this method. Phenylenes such as biphenyl, *m*- and *p*-terphenyl were used as arene reactants. The carbonyl reactants were 1,1,1-trifluoroacetone (TFAc), 2,2,2-trifluoroacetophenone (TFAp), 4-piperidone and derivatives of these.

The Friedel-Crafts type polyhydroxyalkylation reaction proceeds in two steps, both of which are electrophilic aromatic substitutions (**Scheme 6**). The relative rate of these two steps depends on the acidity of the super acid, the electrophilicity of the carbonyl reactants and the nucleophilicity of the aromatic reactants.[144] In the reaction between non-activated aromatic compounds such as biphenyl and terphenyl with TFAp and TFAc in a mixture of TFSA and dichloromethane (DCM), the first step is slower than the second one and is therefore the rate-determining step of the reaction (**Scheme 6**). Thus, a small excess of the carbonyl compounds would increase the rate of this step, resulting in acceleration and dramatic enhancement of the overall polymerization rate. However, too high excess may lead to side reactions and cross-linking.[144] The excess of carbonyl compounds in the synthesis of PAAs was here kept at 10 - 30 mol%.

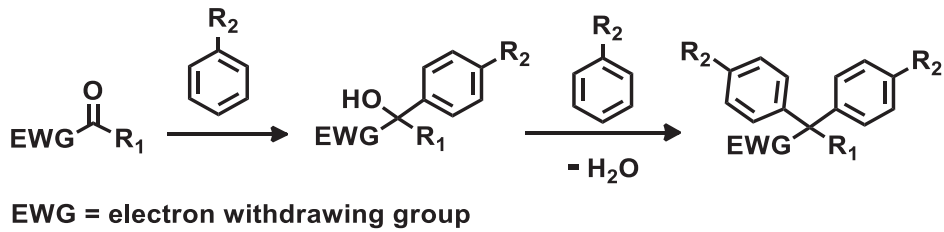

Scheme 6. Mechanism of a Friedel-Crafts type polyhydroxyalkylation reaction.

The solvent used was a mixture of TFSA and DCM. In some cases, a small amount of TFA was also added.[145] The hydrophilicity and acidity of the mixture of solvents can be tuned by adjusting the ratio of TFSA and cosolvents. Choosing an appropriate solvent mixture is one of the major challenges for polyhydroxyalkylation reactions as the solubility of the reaction components is usually very different and can change during the course of the reaction. Since a stoichiometric ratio is not required in polyhydroxyalkylations, it was possible to obtain a high molecular weight polymer even when the aromatic monomers had low solubility in the reaction medium. However, premature precipitation of the resultant polymers often resulted in low molecular weight polymers.

Another challenge in synthesizing the PAAs is the occurrence of side reactions. When the carbonyl monomer contains α-hydrogens, elimination reactions that resulted in dead chain ends were the most prominent side reactions (**Scheme** 7). At the beginning of the polymerization, the molecular weight of the polymer increased with conversion. However, when the polymerization time was kept too long, the dead chain ends produced by elimination accumulated and resulted in a decrease in molecular weight.[84] Therefore, the reaction time must be careful monitored to obtain maximum molecular weight. The reaction temperature was also kept low at 0-20 °C in order to depress the eliminations.

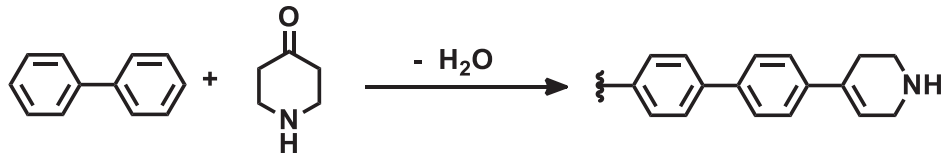

Scheme 7. Elimination at the α-position - a side-reaction in a Friedel-Crafts type polyhydroxyalkylation reaction.

2.1.2. Incorporation of alicyclic quaternary ammonium cations

The greatest challenge in the synthesis of polymers functionalized with alicyclic QA cations is the incorporation of mono- and spirocyclic cations. Menshutkin reactions[146] of polymers containing alkyl halide side chains and monocyclic tertiary amines are the most straightforward and frequently employed methods. However, cationic polymers synthesized in this way still contain β-hydrogens in the side chains that can adapt the anti-periplanar conformation, enabling Hofmann elimination. Connecting the alicyclic QA cations to the polymers at 4- or 3-positions is more desirable but also more challenging. In this thesis work, it was accomplished by first introducing a "precursor" of the alicyclic QA moiety, then transforming that precursor to the desired cation. Two types of precursors were chosen: i) two adjacent bromobenzyl groups and ii) piperidine groups.

Incorporation of the precursors

Spirocyclic QA cations can be synthesized by cycloquaternizations of pairs of adjacent benzyl bromides and monocyclic secondary amines such as pyrrolidine, piperidine and azepane. Pairs of adjacent benzyl bromide were incorporated by bromination of polymers or monomers containing tetramethylphenylene moieties via the free-radical pathway, using *N*-bromosuccinimide (NBS) and azobisisobutyronitrile (AIBN) (**Scheme 8**).[147-150] Due to the delocalization effect

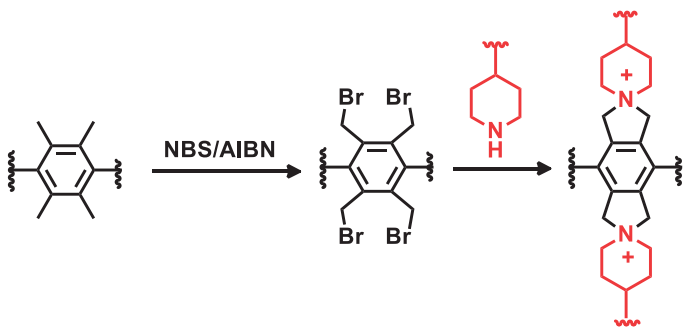

Scheme 8. Radical bromination of a tetramethylphenylene moiety followed by cycloquaternization to give spirocyclic QA cations.

from the aromatic ring, benzylic radicals are stable and are easily formed from methylbenzenes.[151] The radical bromination reactions were highly efficient and proceeded without side reactions. The greatest challenge is ensuring quantitative bromination of all four methyl groups in tetramethylphenylene moieties. Unreactive methyl groups would prevent the cycloquaternization in the next step. Moreover, a residual benzylic C-H bond is weaker than a normal alkyl C-H bond, and prone to for instance oxidation, which leads to a decreased stability of the whole polymer.[152]

The solvent is an important factor that can influence the efficiency of the bromination reaction. Carbontetrachloride is frequently used for radical bromination with NBS and is still irreplaceable in some cases. It is however highly toxic and its usage is restricted. In this work, chloroform was chosen as the solvent for bromination of 1,2,4,5-tetramethylbenzene and chlorobenzene for bromination of PAES.

Another synthetic route to incorporate alicyclic QA cations is via monomers containing secondary or tertiary piperidine groups. These precursor groups were readily transformed further to monocyclic dialkyl piperidinium or spirocyclic ASU, respectively, by quaternization. In this thesis work, six monomers containing secondary or tertiary piperidine groups were employed (**Figure 13**). Four of them, 4,4'-trimethylenedipiperidine, 4,4'-bipiperidine, 4-piperidone and *N*-methyl-4-piperidone are commercially available. The other two were synthesized in-house (**Scheme 9**) by incorporating a piperidine moiety into *m*-terphenyl and TFAp monomers via hydroboration of 4-methylenepiperidine, followed by Suzuki coupling with 5'-bromo-*m*-terphenyl and 4'-bromo-2,2,2-trifluoroacetophenone, respectively.[153]

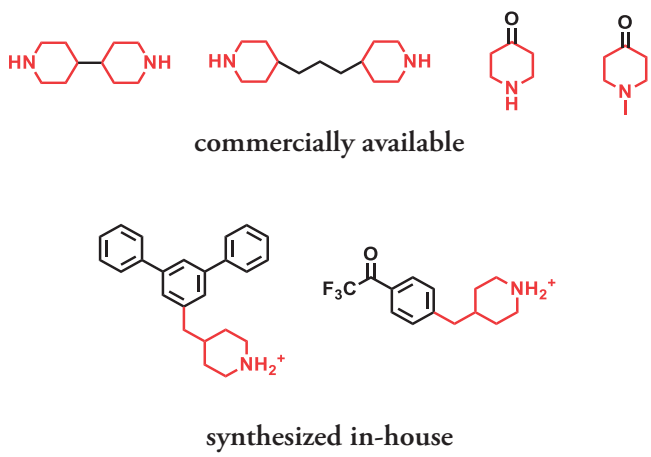

Figure 13. Monomers containing secondary or tertiary piperidine groups.

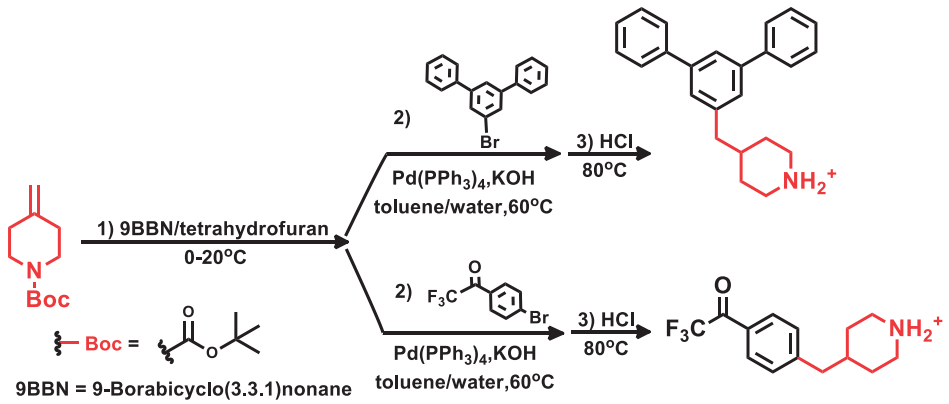

Scheme 9. Incorporation of piperidine moieties in 3 steps: hydroboration (1), Suzuki coupling (2) and deprotection (3).

Quaternization

Alicyclic QA cations were synthesized via *N*-alkylation reactions involving cyclic secondary or tertiary amines and alkyl halides (**Scheme 10**). The alkylation is straightforward and usually proceeds smoothly without side reactions. Reactions between a tertiary amine with alkyl halides (Menshutkin reactions) require no additional reactants. On the other hand, the quaternization of secondary amines requires addition of a base. Here, Hünig's base *N,N*-diisopropylethylamine (DIPEA) was used in most quaternization reactions, except those involving methyl iodide since it can react with DIPEA.[154] For quaternization reactions with methyl iodide, one of the inorganic bases $CaCO_3$ or K_2CO_3 was used.

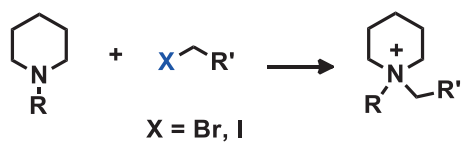

Scheme 10. *N*-alkylation of a cyclic tertiary amine (Menshutkin reaction).

In the present thesis work, the term "cycloquaternization" is used to refer specifically to the reactions between secondary piperidine rings and α,ω-dibromoalkanes. The reaction proceeds via two consecutive nucleophilic attacks; the first one is intermolecular, the second intramolecular (**Scheme 11**). The main drawback of this synthetic pathway is the risk of side reactions that lead to crosslinking. In order to prevent crosslinking, the concentration of the reactants was kept low. The rate of the intramolecular reaction remained unchanged while the intermolecular reaction rate decreased with the concentration. Therefore, the low concentration impeded the intermolecular side reactions and minimize the risk of crosslinking. The solvent also

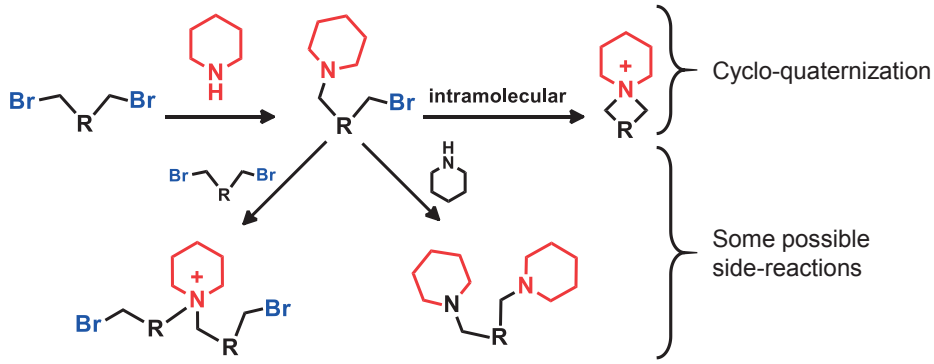

Scheme 11. Cycloquaternization reaction and some possible side-reactions.

had to be carefully chosen to ensure the homogeneity of the reaction mixture. If one of the reactants precipitated, its local concentration would change, leading to an increased risk of side reactions and cross-linking. In many cases, the use of one solvent is not sufficient because of the change in solubility of the compounds during the course of the reaction. In these cases, a mixture of solvents was employed. For example, the PAAs containing protonated secondary piperidine moieties were soluble in DMSO but had low solubility in NMP. However, when the polymers were deprotonated by DIPEA, they became insoluble in DMSO but remained soluble in NMP. Therefore, a mixture of NMP and DMSO was used for the cycloquaternization of these polymers. Likewise, mixtures of *N,N*-dimethylformamide and water were employed for polymerization of the spiro-ionenes.

2.1.3. Characterization

Nuclear magnetic resonance spectroscopy

Nuclear magnetic resonance (NMR) spectra of the synthesized monomers and polymers were obtained using a Bruker DRX400 spectrometer. ^{1}H NMR spectra were obtained at 400 MHz and ^{13}C NMR at 100 MHz. The solvents used were DMSO-d_6 (δ = 2.50 ppm), $CDCl_3$ (δ = 7.26 ppm) and D_2O (δ = 4.79 ppm). In some cases, TFA was added to shift the signal of residual water in order to reveal the compound signals originally overlapped with water. TFA also enhanced the dissolution of the cationic polymers in DMSO-d_6.

Size-exclusion chromatography

Size-exclusion chromatography (SEC) is a method to separate and analyze molecules in solution according to their size.[155] When the polymer solution passes through the size-exclusion column, the smaller molecules enter the pores of the adsorbent packed

inside the column and are thus eluted later than the bigger molecules. The eluent then passes through a detector and the signal intensity is plotted as a function of the elution time (**Figure 14**). A calibration curve is prepared from elution time of standard samples of known molecular weight. The molecular weight of the analyzed sample is determined by comparing its elution time with the calibration curve (**Figure 14**). Here, SEC was employed to determine the molecular weights and polydispersity index (PDI) of unmodified PAES (before radical bromination). A 3 wt% solution of PAES in chloroform at room temperature was passed through a series of three Shodex columns (KF-805,-804, and -802.5) at a rate of 1 ml min^{-1}. The detector was a refractive index detector and the standard consisted of four low polydispersity polystyrene (PS) standards with molecular weights M_n= 650, 96, 30 and 3.18 kg mol^{-1}.

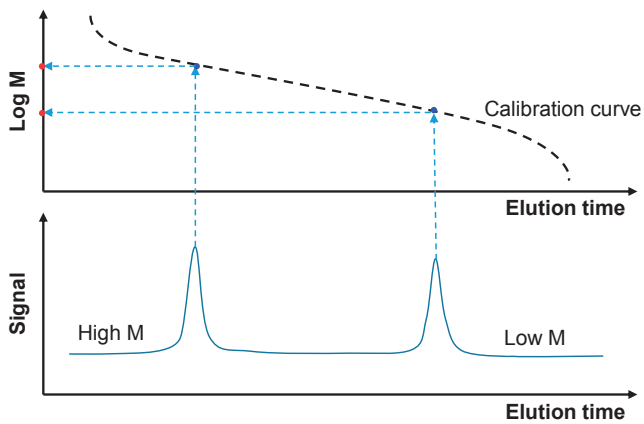

Figure 14. An illustration of the SEC profile of a polymer sample containing two molecular weight fractions.

Intrinsic viscosity

Due to instrument limitations, it was not possible to analyze the polymers that were insoluble in both chloroform and tetrahydrofuran by SEC. In these cases, dilute solution intrinsic viscosimetry was employed to give some indication about the molecular weight of the polymers.[155] Depending on the solubility, they were dissolved in either water or DMSO. LiBr was added to prevent the polyelectrolyte effect. The temperature was kept constant throughout the experiments using a water bath. The elution time through an Ubbelohde viscometer of polymer solutions at different concentrations (t_{sample}) and blank solutions (t_{blank}) was used to calculate the inherent (η_{inh}) and reduced (η_{red}) viscosities according to:

$$\eta_{inh} = \frac{\ln\left(\frac{t_{sample}}{t_{blank}}\right)}{C}$$

$$\eta_{red} = \frac{\frac{t_{sample}}{t_{blank}} - 1}{C}$$

The intrinsic viscosity ([η]) was calculated as the average of the intersections of the linear regressions of η_{inh} and η_{red} with the *y*-axis.[156]

2.2. Membrane preparation and characterization

2.2.1. Membrane preparation and morphology

Membrane preparation

The HEMs were prepared by casting from 5 wt% solutions of the corresponding polymers in NMP or DMSO at 80-85 °C. The membranes were exchanged to bromide and hydroxide form by immersion in 1 M aq. NaBr and NaOH solutions, respectively. Due to their high IEC, spiro-ionenes (**Figure 10**) were water-soluble and had to be blended with a commercially available polybenzimidazole PBI-OO (**Figure 15**) to form HEMs. Blends of 70-80 wt% spiro-ionene **2** (**Figure 10**) with PBI-OO were dissolved in DMSO to give 5 wt% solutions. HEMs were cast from these solutions at 65-80 °C and the resulting membranes were treated with 0.5 M aq. KOH to yield water-insoluble HEMs. The membranes were soluble in DMSO before the treatment with KOH solution but became insoluble afterwards due to the formation of ammonium-imidazolate complexes (**Figure 15**).

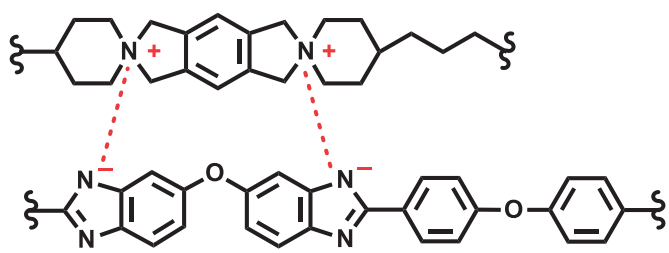

Figure 15. The ammonium-imidazolate complex presumably formed in the blend of spiro-ionene **2** and PBI-OO.

Ion exchange capacity

The IEC of HEMs is an important property that affects both the water uptake and hydroxide conductivity. The IEC value represents the number of ions that can be exchanged in the polymeric membrane and is usually expressed as milliequivalents of ions per gram polymer (meq. g^{-1}). The IEC of HEMs (IEC_{OH}) were not determined directly from acid-base titration because the reaction of the hydroxide counter ions with CO_2 and the potential degradation caused by the hydroxide ions could decrease the accuracy of the results. Instead, IEC_{OH} was determined indirectly from the IEC of the corresponding membranes in bromide form (IEC_{Br}). IEC_{Br} was obtained from Mohr titration. The membrane samples (approximately 0.03-0.06 g) in their bromide form were dried in a vacuum oven (50 °C) for at least 2 days and weighed to obtain the dry weight. Afterwards, they were immersed in 0.2 M aq. $NaNO_3$ solution for 48-240 h and the resulting solutions were titrated with 0.01 M aq. $AgNO_3$ solution. IEC_{OH} was then calculated as:

$$IEC_{OH} = \frac{IEC_{Br}}{1 - \frac{IEC_{Br}(M_{Br^-} - M_{OH^-})}{1000}} = \frac{IEC_{Br}}{1 - 0.0629 \times IEC_{Br}}$$

Small angle X-ray scattering

As mentioned above, membrane phase separation is important for a high hydroxide conductivity. The extent of phase separation was investigated by small angle X-ray scattering (SAXS).[157-158] The membrane samples were irradiated with X-ray and the scattering at small angles (usually < 10°) was detected by a detector (**Figure 16**). The intensity of the scattering can be plotted as a function of the scattering vector (q) (**Figure 17**), which is derived from the scattering angle (θ) and the wavelength of the X-ray (λ) according to:[159]

$$q = \frac{4\pi}{\lambda} sin\theta$$

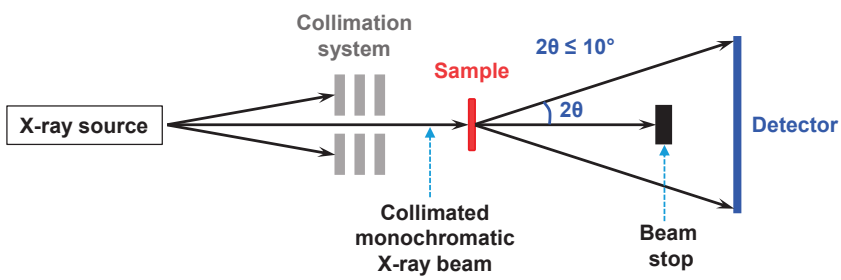

Figure 16. Schematic illustration of a SAXS system

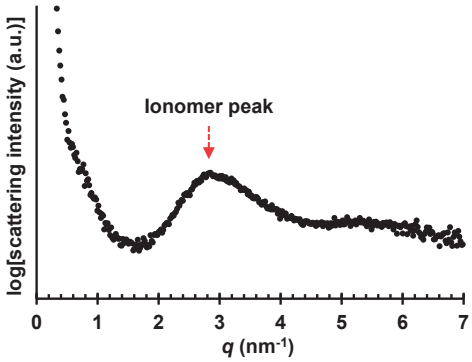

Figure 17. SAXS profile of an IEM with the ionomer peak clearly visible.

If the measured membrane is phase-separated, the difference in electron density of the different phases gives rise to an angular distribution of the scattering. For an IEM, this gives rise to an ionomer peak, indicating the formation of ionic clusters. The maximum of the ionomer peak is correlated to the characteristic separation length (*d*), which is the average length between the ionic clusters, according to:[160-161]

$$d = \frac{2\pi}{q_{max}}$$

In this thesis, SAXS measurements in the q-range 0.14-8.0 nm^{-1} were conducted for AEMs in bromide form, using a SAXSLAB SAXS instrument, from JJ X-ray Systems Aps (Denmark) equipped with a Pilatus detector. The radiation was Cu K_α with wavelength λ =1.542 Å.

2.2.2. Water uptake and hydroxide conductivity

Water uptake

The water uptake (WU) of the HEMs at different temperatures was determined as:

$$WU = \frac{W' - W}{W} \cdot 100\%$$

Here, W is the dry weight obtained after drying the membrane samples in a vacuum oven at 50 °C, and W' is the wet weight of the membrane samples, obtained after immersion at the predetermined temperature. The excess water on the surface was gently removed by tissue paper. Notably, the dry weight in hydroxide form is difficult to obtain due to the risk of carbonation with CO_2 and of degradation when the hydration number decreases. The dry weight of the HEMs was therefore recalculated from the dry weight of the corresponding AEMs in the bromide form

(W_{Br}) and their IEC, assuming quantitative conversion in ion exchange from bromide to hydroxide according to:

$$W = W_{Br} - \frac{W_{Br} \cdot IEC_{Br} \cdot (M_{Br} - M_{OH})}{1000} = W_{Br} - \frac{W_{Br} \cdot IEC_{Br} \cdot 62.9}{1000}$$

Hydroxide Conductivity

The hydroxide conductivity of HEMs in the temperature range -20 – 80 °C was determined under fully hydrated conditions by electrochemical impedance spectroscopy (EIS),[131] using a Novocontrol high resolution dielectric analyzer V 1.01S. The membrane samples were assembled between 2 electrodes in a closed cell (**Figure 18**) to maintain the fully hydrated condition and to avoid contact with CO_2 in air. An alternating current with a magnitude of 50mV and frequency varied between 10^0-10^7 Hz was applied while the cell was kept at a predetermined temperature. The conductivity was plotted against the frequency and the plateau values were taken as the hydroxide conductivity of the sample at that temperature (**Figure 19**).

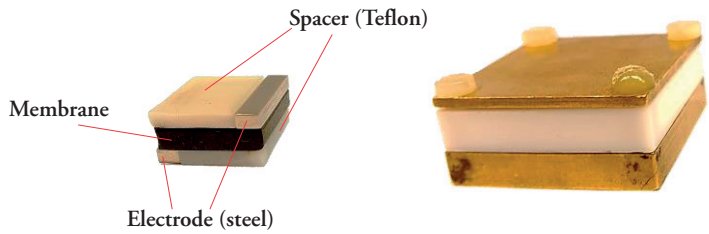

Figure 18. An HEM assembled for EIS measurements (left) and the closed cell (right) that covers the whole assembly to maintain the fully hydrated condition and to avoid contact with CO_2. The thin membrane is here replaced by a thick piece of rubber (black) for clarity.

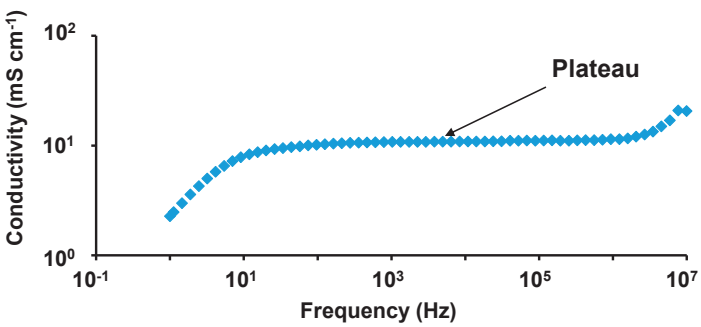

Figure 19. The conductivity as a function of frequency at constant temperature showing a clear plateau between 10^1-10^6 Hz.

2.2.3. Thermal and alkaline stability

Thermal stability

The thermal stability of the AEMs in bromide form in N_2 atmosphere was measured by thermogravimetric analysis (TGA), using a TA Instruments Q500 Analyzer. The samples were first pre-dried at 100-120 °C to remove residual solvents and then heated from 50 °C to 600 °C at a heating rate of 10 °C min^{-1}. The weight of the samples was measured continuously while increasing the temperature and the thermal decomposition temperature was taken at 5% weight loss ($T_{d,95}$).

Alkaline stability

Figure 20. From left to right: an empty glass pressure tube, a Teflon inner tube, a front seal and an assembled holder for the alkaline stability study.

In order to evaluate the alkaline stability of the HEMs, the membrane samples were first immersed in alkaline solution at a predetermined temperature. Typically, the membrane sample was stored in 1 or 2 M aq. NaOH solution at 20-120 °C. At lower temperature (20-60 °C) the HEMs were immersed directly in alkaline solution in a glass holder. For alkaline stability studies at above 80 °C, glass pressure tubes with custom-made Teflon inner tubes were used (**Figure 20**). The pressure tubes with a safety seal prevent evaporation of water, maintaining the concentration and temperature constant throughout the experiments. The Teflon inner tubes impede the corrosion of the pressure tube caused by direct contact with the highly corrosive alkaline solution. The temperature was kept constant by using an oven or a heated oil bath. Membrane samples were taken out after different periods of time, washed extensively with deionized water and ion-exchanged to bromide form. After drying in a vacuum oven at 50 °C, they were dissolved in DMSO-d_6 and analyzed by ^{1}H NMR spectroscopy. In some cases, TFA was also added to the polymer solutions in order to shift the residual water signal and to protonate any tertiary amine

degradation products, assisting in the elucidation of the extent and the mechanism of degradation.

The alkaline stability study of water-soluble spiro-ionenes were conducted slightly differently. The spiro-ionenes were dissolved in 1 M KOD solution in D_2O. After different periods of time, a portion of the solution was taken and analyzed directly by ^1H NMR spectroscopy.

NMR spectroscopy was chosen for the evaluation of the alkaline stability of the HEMs in this thesis due to the versatility of the technique. NMR spectroscopy does not require much material, is easy to repeat and can detect low degrees of degradation with high accuracy. Furthermore, NMR spectroscopy enables the study of not only the degree but also the mechanism of degradation, as different degradation pathways can give rise to degradation products with varying chemical shifts in NMR spectroscopy. By comparing the signal intensity of each degradation product with that of the original polymer, the degree of degradation by specific pathways was estimated.

3. Summary of appended papers

3.1. Hydroxide exchange membranes based on poly(arylene ether sulfone)s (Paper I)

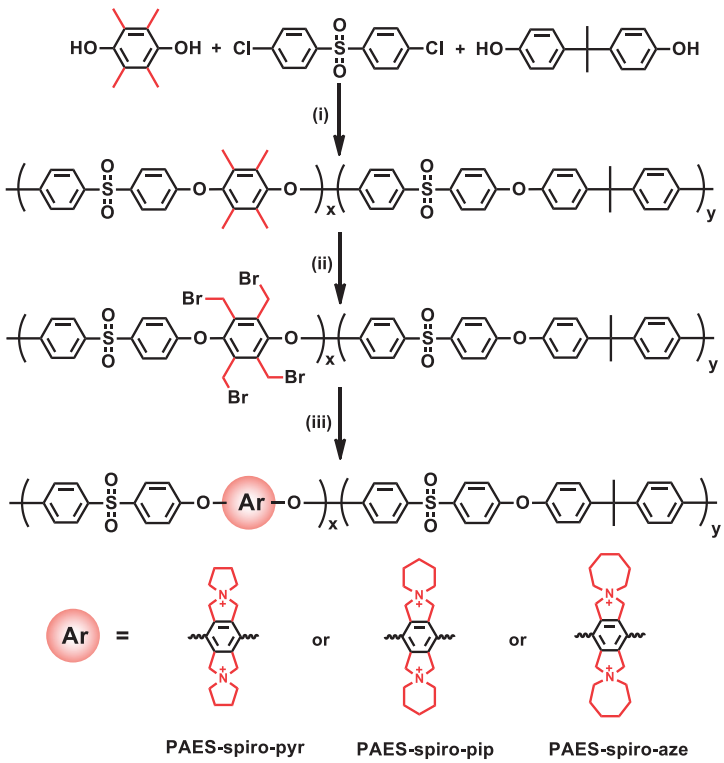

Scheme 12. Synthetic pathways to PAES functionalized with spirocyclic QA cations in 3 steps: polyesterification (i), radical bromination (ii) and cyclo-quaternization (iii).

In the first approach to incorporate the *N*-spirocyclic QA cations into the anion exchange membrane, a PAES backbone was employed. Even though the PAES backbone has a tendency to degrade in alkaline medium, this approach has a clear advantage in its straightforward synthesis. PAESs functionalized with *N*-spirocyclic

QA cations were successfully synthesized in three steps, where the first two, polyetherification and radical bromination, followed a previously reported procedure.[162-164] The last step was cycloquaternization, using the cyclic secondary amines pyrrolidine, piperidine and azepane, to give three cationic polymers. The polymers were designated **PAES-spiro-*x***, where *x* = pyr, pip and aze, respectively (**Scheme 12**). The IEC values determined by titration of the AEMs based on these polymers in bromide form were 1.62, 1.51 and 1.49 meq. g^{-1}, which corresponded to IEC values of the HEMs of 1.80, 1.67 and 1.64 meq. g^{-1}, respectively (**Table 2**).

SAXS profiles of all HEMs based on **PAES-spiro-*x*** polymers displayed clear ionomer peaks at the same q_{max} ~1.3 nm^{-1}, corresponding to a characteristic distance *d*~ 4.8 nm (**Figure 21**). On the other hand, the scattering intensity increased with decreased ring size, probably because the increased electrostatic shielding effect of a larger ring impeded the clustering and scattering efficiency of the clusters.

Table 2. Properties of HEMs based on **PAES-spiro-*x***

HEM	IEC (meq. g^{-1})		WU [b]	σ[b]	$T_{d,95}$[c]
	theoretical [a]	titrated	(wt%)	(mS cm^{-1})	(°C)
PAES-spiro-pyr	1.76(1.98)	1.62(1.80)	53	110	308
PAES-spiro-pip	1.72(1.92)	1.51(1.67)	53	53	309
PAES-spiro-aze	1.68(1.87)	1.49(1.64)	45	24	274

[a] Calculated from the chemical structure of the polymers in the bromide form, (values for the hydroxide form within parentheses).[b] Measured at 80 °C in the hydroxide form under fully hydrated conditions (immersed).[c] Measured by TGA under N_2 at 10 °C min^{-1}.

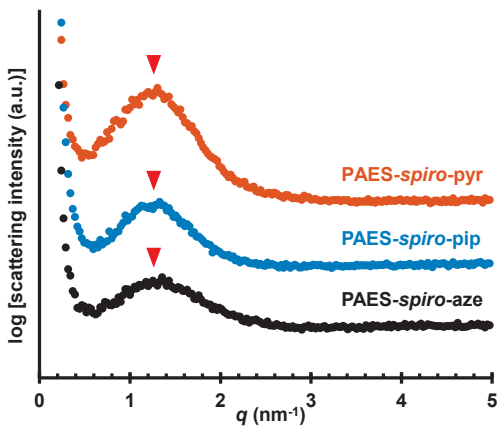

Figure 21. SAXS profiles of **PAES-spiro-x** AEMs in bromide form.

As expected, both water uptake and conductivity increased with decreased ring size and increased temperature (**Figure 22**). The increase in water uptake and conductivity was possibly a combined effect of both higher IEC and more efficient ion clustering of the smaller ring. At 80 °C, the hydroxide conductivity of HEMs based on **PAES-spiro-pyr**, **-pip** and **-aze** reached 110, 53 and 24 mS cm^{-1}, respectively.

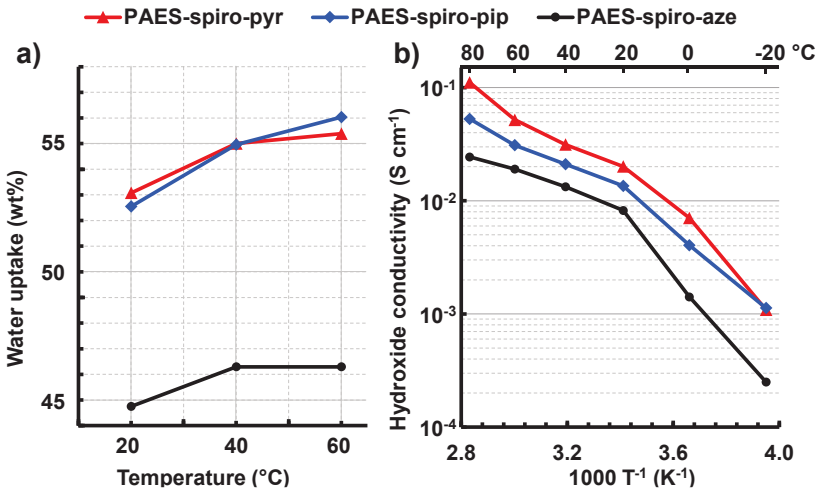

Figure 22. Water uptake of fully hydrated HEMs based on **PAES-spiro-*x*** as a function of temperature (a) and hydroxide conductivity of these HEMs as a function of T^{-1} (b).

Both the thermal and chemical stability of the PAES membranes functionalized with spirocyclic QA cations were significantly improved in comparison with the corresponding PAESs functionalized with BTM. The former had a thermal decomposition temperature $T_{d,95}$ between 274 and 309 °C, while decomposition occurred between 233 and 269 °C for the latter. [163-164] Furthermore, the **PAES-spiro-*x*** membranes showed no significant degradation after 168 h storage in 1 M aq. NaOH solution at 20 °C as no change in the ^{1}H NMR spectra was observed. After 168 h storage at 40 °C, ^{1}H NMR spectra of all three **PAES-spiro-*x*** HEMs showed new signals at 4.5 ppm, corresponding to benzyl protons in benzyl alcohols, the products of nucleophilic substitution at the benzyl position of the spirocyclic cations (**Figure 23**).

Comparing the intensity of these signals with the original benzyl protons signal at 4.8 ppm, the ionic loss was estimated to 5% for all HEMs. In contrast, under the same conditions, HEMs based on PAES functionalized with BTM presented ~80% loss of the QA groups.[163-164] The ionic loss of the PAES-spiro membranes increased sharply when the temperature was raised to 60 °C. In addition, the polymer backbones also decomposed as indicated by the appearance of new signals in the

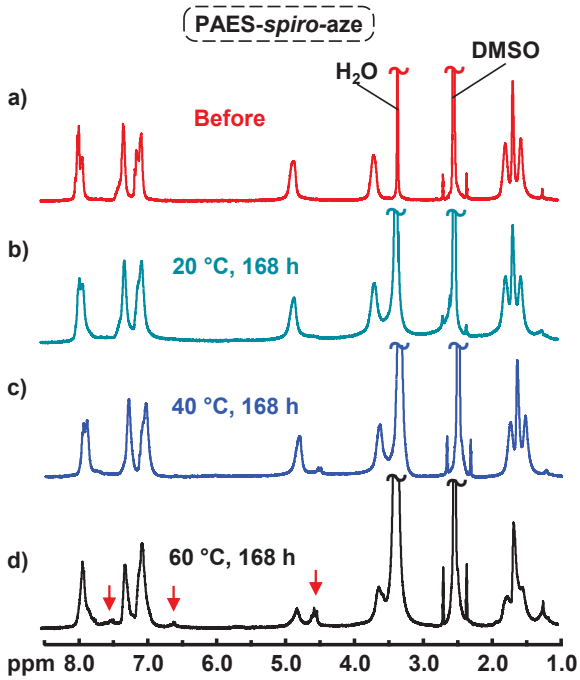

Figure 23. ^{1}H NMR spectra of **PAES-spiro-aze** before (a) and after 168 h storage in 1 M NaOH solutions at 20 (b), 40 (c) and 60 °C (d).

aromatic region (6.5-8 ppm). The membranes also became more brittle and were broken into small pieces, which suggested a decrease in molecular weight due to chain cleavage, probably at the aryl ether bonds.

3.2. Spiro-ionenes (Paper II)

The PAESs have low alkaline stability due to the presence of both strong electron withdrawing groups and aryl ether bonds. In our first attempt to overcome this issue, aryl ether-free spiro-ionenes were designed, synthesized and investigated as potential anion-conducting polymers. In fact, spiro-ionenes are not a new type of material. The synthesis of similar polymers was reported by Müllen et al. already in 1990,[138] but only the solubility and the thermal properties were studied. In this work, two spiro-ionenes were synthesized by polycondensation of commercially available dipiperidines, 4,4'-bipiperidine and 4,4'-trimethylenedipiperidine, with tetrakis(bromomethyl)benzene (**Scheme 13**). The cyclo-polycondensation reaction was efficient and produced the polymers in quantitative yield under mild conditions in short time. The key challenge in synthesizing these polymers was the selection of

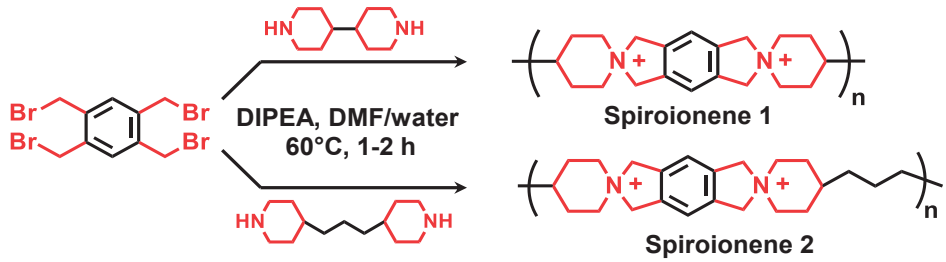

Scheme 13. Synthetic pathway to spiro-ionenes via cyclo-polycondensation.

an appropriate solvent system to avoid precipitation and gelation. In addition, the concentration was kept low (~ 3 - 3.6 wt%) to suppress intermolecular crosslinking. The resulting spiro-ionenes had good solubility in water and gave high-resolution ^{1}H NMR spectra in D_2O. Thus, the molecular weight could be estimated by comparing the chain end group signals with the repeating units signals in their ^{1}H NMR spectra.

The spiro-ionenes had excellent thermal and chemical stability. The thermal decomposition temperature $T_{d,95}$ of spiro-ionenes **1** and **2** was 336 and 318 °C, respectively. The higher $T_{d,95}$ value of spiro-ionene **1** was induced by the stiffer structure and higher aromaticity. The alkaline stability of the spiro-ionenes was studied by H^1 NMR spectroscopy of polymer solutions in 1 M KOD/D_2O at 80 and 120 °C. Both polymers showed no detectable sign of degradation after 672 h at 80 °C (**Figure 24**). Especially, spiro-ionene **2** did not degrade even after extending the alkaline stability study to 1896 h. Still, when the temperature was raised to 120 °C, both polymers degraded via ring-opening nucleophilic substitution as indicated

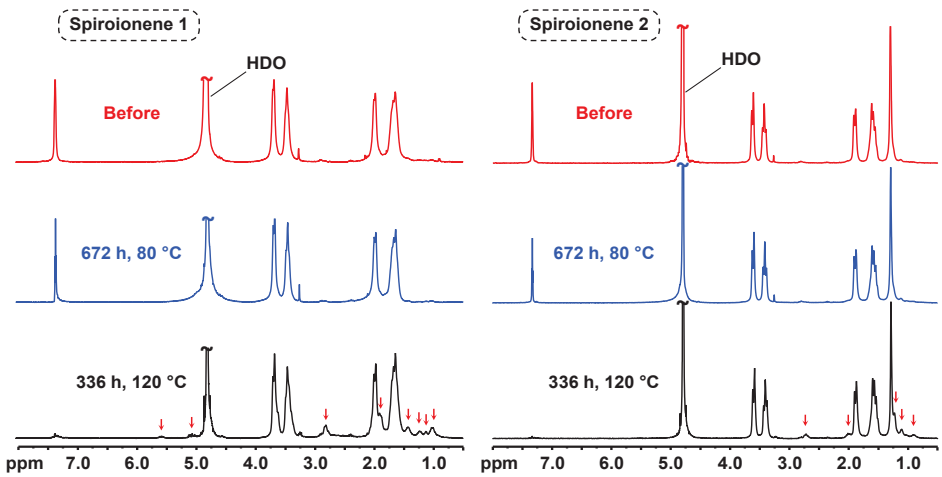

Figure 24. ^{1}H NMR spectra of the spiro-ionenes before and after the alkaline stability test at 80 and 120°C

by the appearance of new signals at ~ 2.7-2.8 and ~1.9-2.0 ppm, which corresponded well to α-protons in *N*-benzylpiperidine groups. Comparing the intensity of these signal with the original polymer signals at ~3.6-3.7 ppm, the degree of degradation via this pathway after 336 h storage for spiro-ionenes **1** and **2** were estimated to 15 and 10%, respectively. In addition, spiro-ionene **1** also degraded via Hoffman elimination in the 6 membered ring, giving rise to new alkene and alkenyl signals at ~ 5.5 and 5.0 ppm. The degree of degradation via this pathway was estimated to be ~10%. The flexible trimethylene spacer between two rigid fragments of spiro-ionene **1** was probably the cause of the remarkably higher alkaline stability, as it can greatly facilitate ring strain relaxation and help mitigate the distortion of the 6-membred ring system.

The spacer also promoted phase separation and formation of ion clusters. SAXS profiles of spiro-ionene **2** equilibrated at 75% relative humidity (RH) showed a weak ionomer peak at $q_{max} \sim 4.8$ nm^{-1}, corresponding to a characteristic distance of $d \sim$ 1.3 nm. Meanwhile, spiro-ionene **1** showed no distinct ionomer peak under the same conditions (**Figure 25**).

Due to the high IEC, both spiro-ionenes were water soluble. In order to prepare HEMs, blends of spiro-ionene **2** and PBI-OO were cast from DMSO solutions. After alkaline treatment, a fraction of the imidazolium groups in PBI-OO was deprotonated and could form ammonium-imidazolate complexes together with the QA cations of spiro-ionene **2** (**Figure 15**), giving rise to water-insoluble HEMs. The membranes were designated **S*x*P*y***, where *x* is the weight percentage of spiro-ionene **2** and *y* is the weight percentage of PBI-OO. The water uptake and hydroxide conductivity of these HEMs were controlled by varying the weight percentage of spiro-ionene **2** in the blend (**Figure 26**). Out of the three blend membranes prepared in this project, **S70P30** had the highest hydroxide conductivity of 118 mS cm^{-1} and

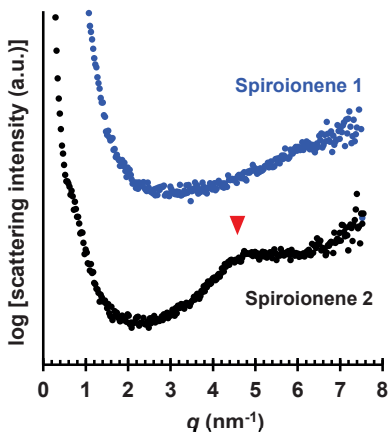

Figure 25. SAXS profiles of the spiro-ionenes equilibrated at 75% RH.

the lowest water uptake of 222 wt% at 80 °C. The water uptake increased drastically when the weight percentage of spiro-ionene **2** increased. **S80P20** reached a high water uptake of 800 wt% at 80 °C. Consequently, the hydroxide conductivity decreased to 66 mS cm^{-1} due to the dilution effect (**Figure 26**).

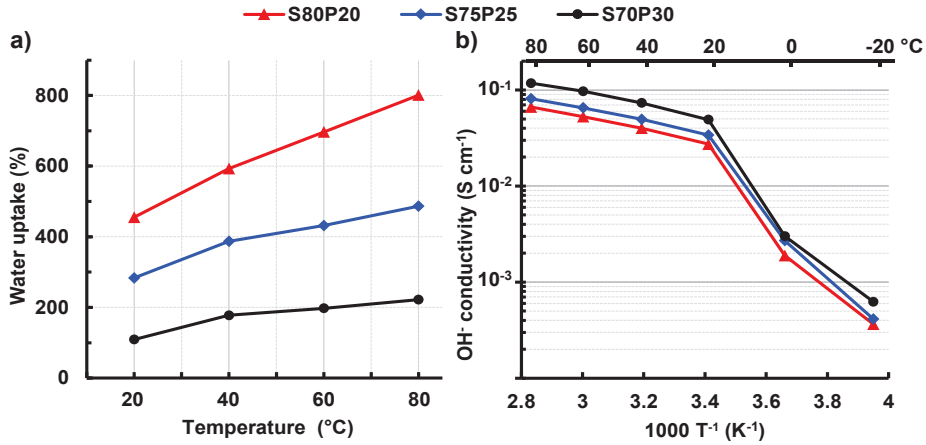

Figure 26. Water uptake of fully hydrated blend membranes **SxP*y*** in hydroxide form as a function of temperature (a) and hydroxide conductivity of these HEMs as a function of T^{-1} (b)

3.3. Hydroxide exchange membranes based on poly(arylene alkylene)s (Paper III-V)

The cationic polymers with the spirocyclic QA cations directly incorporated into the polymer backbone have a severe disadvantage: the degradation of the QA cations can lead to backbone cleavage and decreased mechanical strength. Due to the unique ring fusion structure of the spiro-ionenes, the degradation of these polymers should only cause ring opening without complete cleavage of the backbone and decrease of molecular weight. However, it still leads to a less rigid backbone and to deteriorated mechanical properties. A better strategy would be to incorporate alicyclic QAs as side chains of an aryl ether-free backbone. There are only a few methods to synthesize ether-free backbones. Throughout this section, the selected polymer backbones belonged to the PAA family and were synthesized by Friedel-Craft type polyhydroxyalkylations. The piperidine or *N*-methylpiperidine groups, the precursors of alicyclic piperidinium cations, were smoothly incorporated by choosing a monomer already bearing these groups. The resulting precursors were readily transformed to monocyclic *N,N*-methylalkyl piperidinium, or to spirocyclic ASU

cations by quaternization using alkyl halides or cycloquaternization using α,ω-dibromoalkanes, respectively.

3.3.1. Effect of cations (Paper III-IV)

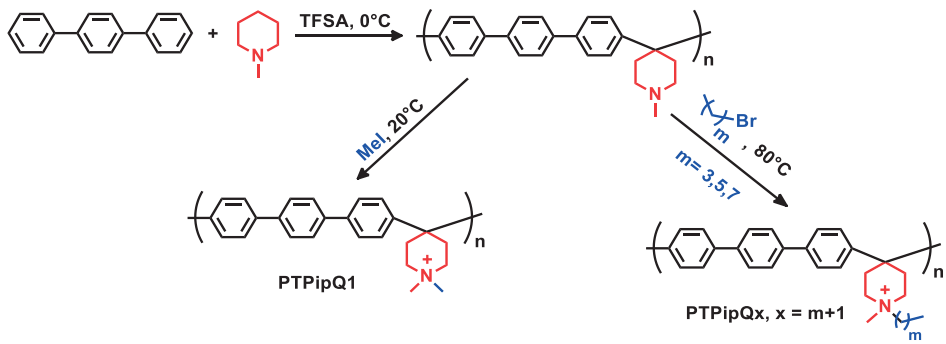

Scheme 14. Synthetic pathways to **PTPipQx** polymers

The first approach was focused on poly(terphenyl *N,N*-methyl alkyl piperidinium)s, a subclass of PAA with *N,N*-methylalkyl piperidinium cations directly attached to a polymer backbone (**Figure 9b**). The synthesis of the precursor polymer **PTPip** was straightforward from commercially available monomers *N*-methyl-4-piperidone and *p*-terphenyl (**Scheme 14**). A quaternization reaction of **PTPip** with methyl iodide, butyl bromide, hexyl bromide and octyl bromide resulted in a series of cationic polymer with alkyl pendant chains of varied length. These polymers were designated **PTPipQ*x***, where *x* corresponds to the number of carbon atoms in the alkyl extenders.

When varying the length of the alkyl extender chain, one can monitor the IEC, WU and conductivity of the HEMs. The water uptake decreased with increasing extender chain length, mainly due to an increased IEC. At 80 °C, the water uptake values were 404, 290, 171 and 79% for **PTPipQ1**,-**Q4**, -**Q6** and -**Q8**, respectively (**Table 3**). The longer extender chain also promoted phase separation and ion cluster. When studied by SAXS, **PTPipQ1**, with the shortest extender, displayed no distinct scattering peaks. Meanwhile, **PTPipQ4**, - **Q6**, and - **Q8** presented clear scattering peaks at q_{max} ~ 5.2, 4.6 and 4.1 nm^{-1}, corresponding to characteristic distances of *d* ~1.2, 1.4, and 1.5 nm, respectively. The more efficient phase separation together with a decreased dilution effect (lower water uptake) resulted in higher hydroxide conductivity when the alkyl extender chain was extended from methyl to hexyl. The hydroxide conductivity of **PTPiPQ1** and -**Q6** membranes at 80 °C was 89 and 111 mS cm^{-1}, respectively. However, the hydroxide conductivity decreased sharply to 61 mS cm^{-1} when the length of the alkyl extender increased further to eight carbons

Table 3. Properties of the HEMs based on **PTPipQx** polymers

HEM	IEC (mequiv. g^{-1})		WU[b]	σ[b]	$T_{d,95}$[c]	d[d]	Ionic
	theoretical[a]	titrated	(wt%)	(mS cm^{-1})	(°C)	(nm)	loss[e] (%)
PTPipQ1	2.38(2.80)	2.42	404	89	264	4.5	8
PTPipQ4	2.16(2.50)	2.21	290	84	250	1.2	46
PTPipQ6	2.04(2.34)	2.08	171	111	241	1.4	65
PTPipQ8	1.93(2.19)	1.98	79	61	232	1.5	73

[a] Calculated from the chemical structure of the polymers in the Br^- form, (values in hydroxide form within the parentheses). [b] Measured at 80 °C in the hydroxide form under fully hydrated conditions (immersed). [c] Measured by TGA under N_2 at 10 °C min^{-1}. [d] Measured by SAXS in the dry Br^- form. [e] Total ionic loss estimated by comparing the protonated tertiary amine proton signals (above 9 ppm) and the aromatic signals (7.0-8.0 ppm) in ^{1}H NMR spectra of the HEMs after storage in 2 M NaOH aq. solution at 90 °C during 720 h.

(octyl) (**Table 3**), probably due to insufficient formation of a water percolating system caused by an insufficient water uptake. Thus, *N,N*-methylhexyl piperidinium in **PTPipQ6** was the optimum choice of cation in order to obtain HEMs with a high hydroxide conductivity and a reasonable water uptake.

However, the long alkyl extender also led to decreased thermal stability. Hence the thermal decomposition temperature $T_{d,95}$ decreased with increased alkyl extender length (**Table 3**). In addition to the thermal stability, the thermochemical stability of the HEMs under the working conditions of the electrochemical device is a crucial property that affects their performance and lifetime. The QA cations of the HEMs degraded via both direct nucleophilic substitution at α-carbons and Hofmann elimination at β-hydrogens. Both pathways led to ionic loss by formation of tertiary amine products. Upon protonation with TFA, these tertiary amine products induced new signals above 9 ppm, well-separated from the other signals. Meanwhile, the alkenes (degradation products of Hofmann elimination) gave rise to three distinct vinylic protons (-C*H*=CH_2) with signals at 5.0, 5.4, and 6.6 ppm. As a result, the degree of ionic loss, both in total and by Hofmann elimination was estimated by comparing the intensity of the relevant signals with the aromatic signals (**Figure 27** and **Figure 28**).

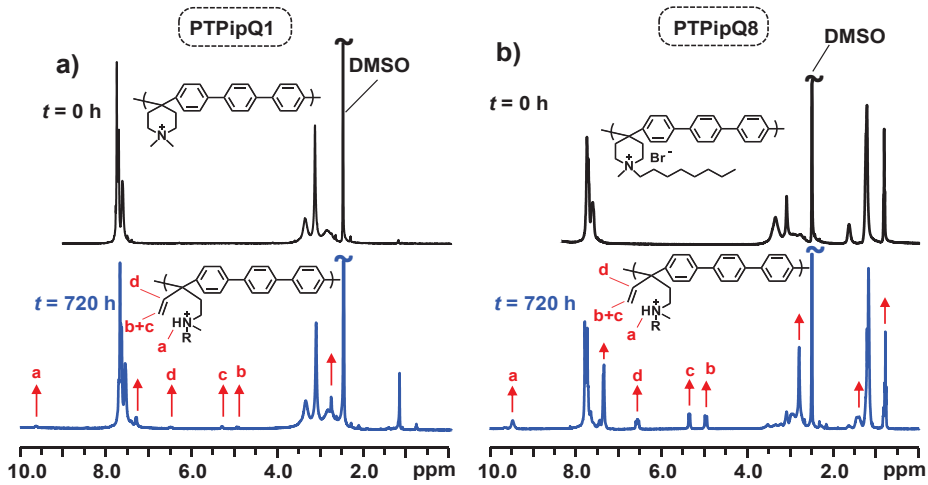

Figure 27. ^{1}H NMR spectra of **PTPipQ1** (a) and **PTPipQ8** (b) recorded in DMSO-d_6/TFA before and after 720 h immersion in 2 M NaOH solutions at 90 °C. TFA was added to shift the water signals. The red arrows mark new signals originating from degradation products.

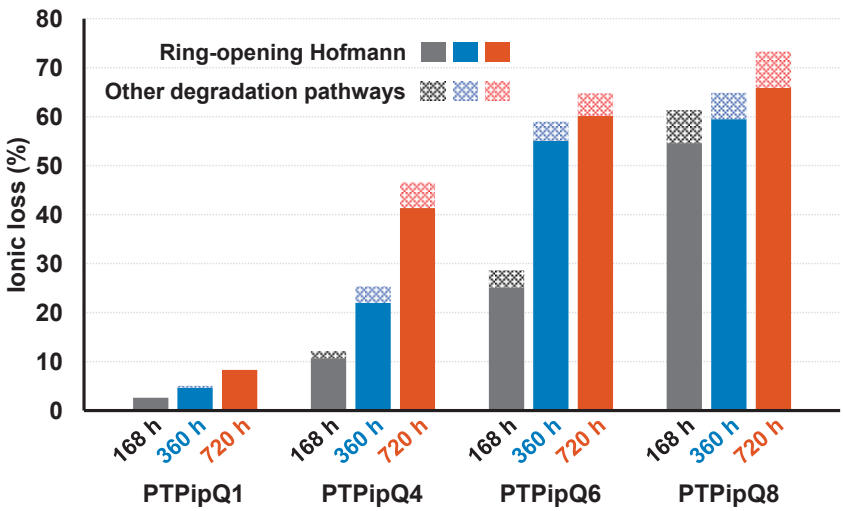

Figure 28. The total ionic loss of the HEMs based on **PTPipQx** polymers after immersion in 2 M NaOH solutions at 90 °C for 168 (black), 360 (blue) and 720 h (red). The solid colored part of the bars display the contribution from ring-opening Hofmann elimination. The patterned parts of the bars show the contribution from other degradation pathways.

The thermochemical stability of poly(terphenyl *N,N*-methylalkylpiperidinium)s followed the same trend as their thermal stability. Amongst the investigated *N,N*-methylalkylpiperidinium cations, DMP was the most stable and *N,N*-methyloctylpiperidinium the least stable in an alkaline environment. After 720 h storage in 2-M NaOH at 90 °C, the total ionic loss of **PTPipQ1**, **-Q4**, **-Q6**, and **-Q8** was 8, 46, 65 and 73%, respectively. Notably, the majority of the ionic loss (90-100%) was the result of ring-opening Hofmann elimination (**Figure 28**). The introduction of long alkyl extenders probably distorted the six-membered ring and restricted ring strain relaxation, thus significantly decreasing the alkaline stability of the alicyclic QA cations. A possible strategy to high-performance PAA-based HEMs would be by combining DMP cations for high thermal and thermochemical stability with partial functionalization, copolymerization or crosslinking to reduce the water uptake and increase the hydroxide conductivity.[165]

According to Marino et al., the spirocyclic ASU cation is even more stable than DMP.[91] In order to incorporate ASU into the PAA backbone, the secondary amine 4-piperidone was employed in the polyhydroxyalkylation together with biphenyl. The secondary piperidine ring in the precursor underwent cycloquaternization with dibromopentane to form the desired ASU QA cations, directly attached to a PAA backbone. Furthermore, to lower the IEC and prevent excessive water uptake of the resulting HEM, either TFAc or TFAp comonomers were introduced together with piperidone as comonomers during the polymerization reaction. The resulting polymers were designated **P6Me-*z*** and **P6Ph-*z***, where *z* is the titrated IEC of the HEMs based on these polymers (**Scheme 15**).

When attached directly on the PAA backbones, the alkaline stability of ASU was lower than for DMP, but still higher than for the other monocyclic QA cations (**Figure 29**). After 720 h of storage in 2 M NaOH at 90 °C, the total ionic loss of these HEMs exceeded 20%. The Hofmann elimination at the piperidine ring directly attached to the backbone (Pi1) and at the pendant piperidine ring (Pi2) gave

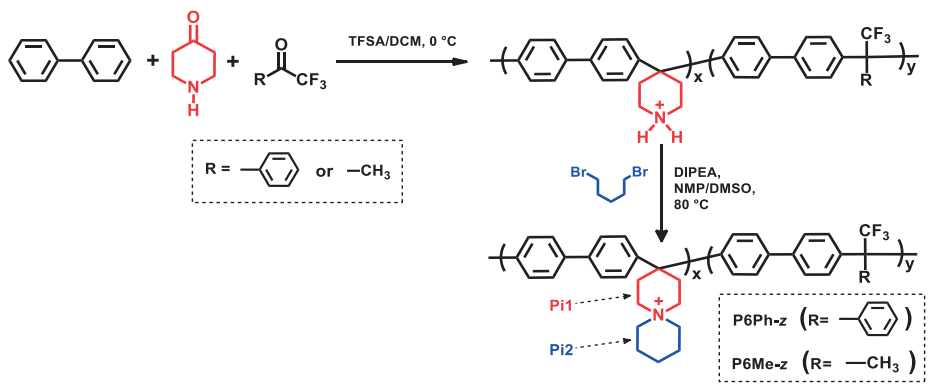

Scheme 15. Synthetic pathways to **P6Me-*z*** and **P6Ph-*z***

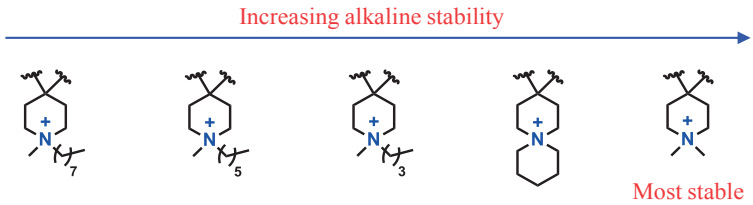

Figure 29. The relative alkaline stability of alicyclic QA cations directly attached to PAA backbones.

rise to two distinct sets of ^{1}H NMR signals (**Figure 30**). According to the relative intensity of these signals, Pi1 rings were more susceptible to Hofmann elimination, suggesting that the direct attachment to the polymer backbone destabilized the piperidinium cations. One possible explanation to this behavior is that the bulky and rigid polymer backbone severely distorted the bond angles in the piperidine ring, thus preventing conformational relaxation and increasing the energy level of the piperidinium cations. This reduced the activation energy and facilitated the degradation reactions. The result was consistent with the previous findings concerning the alkaline stability of spiro-ionenes.[166] Spiro-ionene **2**, with the flexible spacer that can mitigate the distortion of the ring system, was significantly more stable than the rigid spiro-ionene **1**.

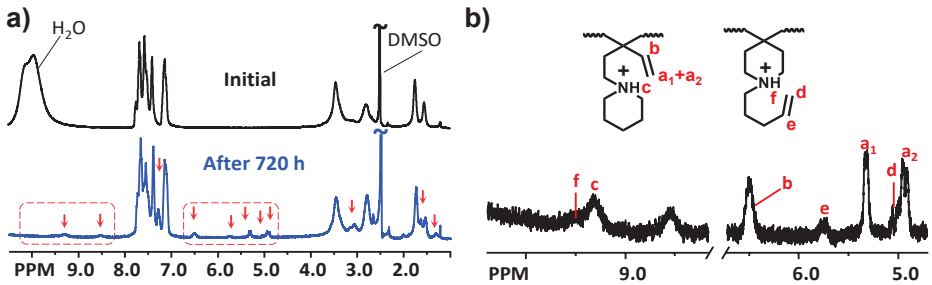

Figure 30. ^{1}H NMR spectra of **P6Ph-1.8** recorded in DMSO-d_6/TFA before and after 720 h immersion in 2 M NaOH solutions at 90 °C (a). TFA was added to shift the water signals. The red arrows point out new signals originating from degradation products. Expansion of the regions between 4.7–6.7 and 8.7–10.4 ppm (marked by red dashed boxes) and possible products from Hofmann elimination of ASU cations are also shown (b).

3.3.2. Effect of spacer and backbone structure (Paper V)

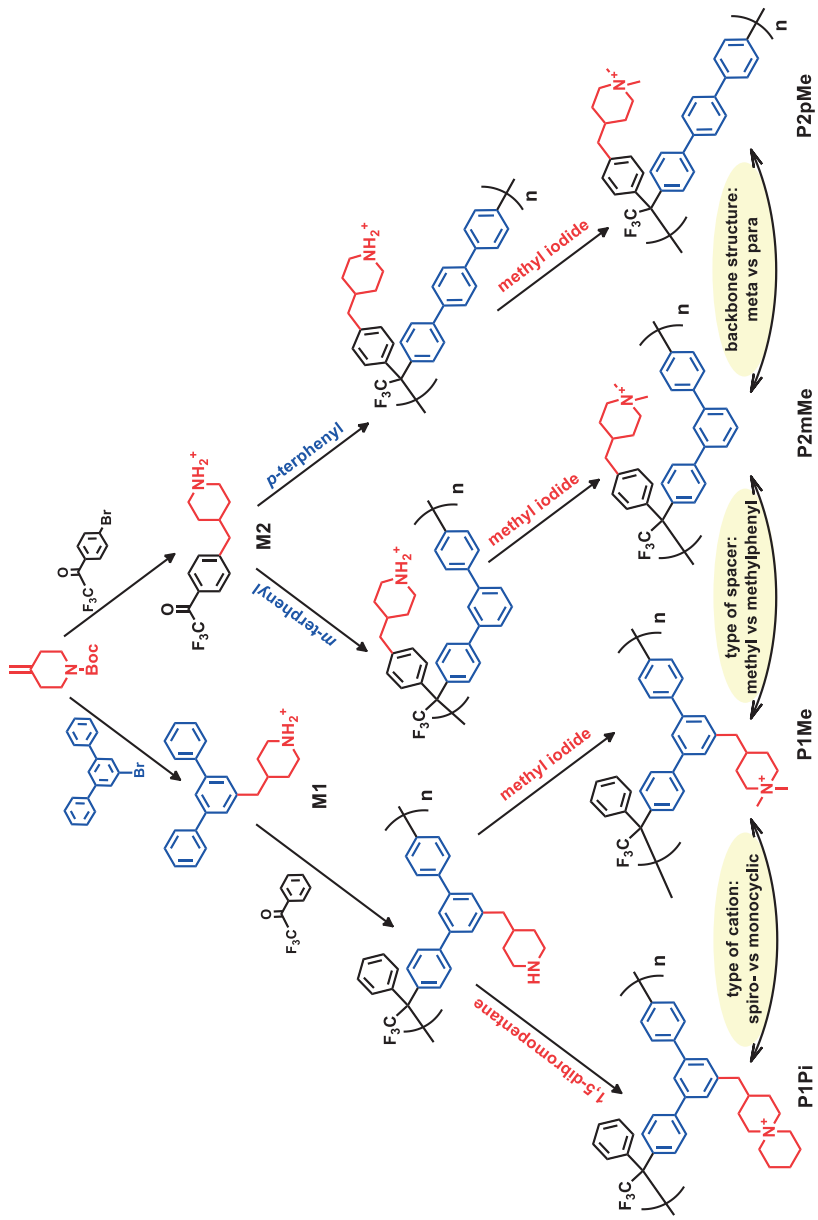

Scheme 16. Synthetic pathways to PAA polymers with alicyclic QA cations attached via spacers.

The placement of the *N*-alicyclic piperidinium cations on the polymer backbone not only destabilized the cations, but also restricted their mobility and prevented the efficient phase separation necessary for high hydroxide conductivity. In order to improve the alkaline stability and hydroxide conductivity of the HEMs, the *N*-alicyclic piperidinium cations ASU and DMP were attached to the poly(arylene alkylene) backbone via a spacer. Initially, two monomers **M1** and **M2** (**Scheme 16**) were synthesized by attaching the 4-benzyl-piperidine moiety to *m*-terphenyl and trifluoroacetophenone, respectively, using Suzuki coupling reactions. Polymerization reactions of these monomers together with suitable comonomers, employing Friedel-Craft type polyhydroxyalkylations, resulted in precursor poly(arylene alkylene)s with piperidine groups attached via methyl or methylphenyl spacers. The backbone structure was also conveniently controlled by the variation of the comonomers. Finally, the piperidine groups of the precursor polymers were converted to DMP or ASU cations by quaternization with methyl iodide or cycloquaternization with 1,5-dibromopentane, respectively. The resultant polymers were designated **P1Pi**, **P1Me**, **P2mMe** and **P2pMe** according to **Scheme 16**. The properties of HEMs based on these polymers are summarized in **Table 4.**

As expected, the attachment of DMP cations to the polymer backbones via the longer methylphenyl spacer instead of a methyl spacer had a positive effect on the hydroxide conductivity. Membrane **P2mMe** and **P1Me** had the same polymer backbone and similar water uptake, but **P2mMe**, which had the methylphenyl spacer reached a hydroxide conductivity of 146 mS cm^{-1} at 80 °C, i.e., 36% higher as compared with **P1Me** at identical conditions. On the other hand, an increase in

Table 4. Properties of the HEMs described in Paper V

HEM	IEC (mequiv. g^{-1})		WU [b]	σ [b]	$T_{d,95}$ [c]	Total ionic loss [d]
	theoretical [a]	titrated	(wt%)	(mS cm^{-1})	(°C)	
P1Pi	1.58(1.75)	1.57	54	58	335	~10% (55%)
P1Me	1.69(1.89)	1.71	99	107	282	<5% (33%)
P2mMe	1.69(1.89)	1.73	103	146	269	<5% (27%)
P2pMe	1.69(1.89)	1.82	73	103	275	<5% (35%)

[a] Calculated from the chemical structure of the polymers in the bromide form, (values for the hydroxide form within the parentheses). [b] Measured at 80 °C in the hydroxide form under fully hydrated conditions (immersed). [c] Measured by TGA under N_2 at 10 °C min^{-1}. [d] Estimated by comparing the protonated tertiary amine proton signals (above 9 ppm) and the aromatic signals (7.0-8.0 ppm) in ^{1}H NMR spectra of the HEMs after storage in 2 M NaOH aq. solution at 90 °C during 720 h, (values for 168 h storage at 120 °C within parentheses).

rigidity of the backbone resulted in decreased water uptake and consequently, decreased hydroxide conductivity. Hence, replacement of the *m*-terphenyl units in **P2mMe** with the stiffer *p*-terphenyl units in **P2pMe** resulted in a drop by ~30% of both the water uptake and the hydroxide conductivity (**Table 4**).

The introduction of spacers also improved the alkaline stability. As estimated by ^{1}H NMR spectroscopy, after 720h of immersion in 2 M aq. NaOH solution at 90 °C, the total ionic loss of **P1Pi** was only 10% (**Figure 31**, **Table 4**). However, HEM functionalized with ASU still showed a lower alkaline stability than those

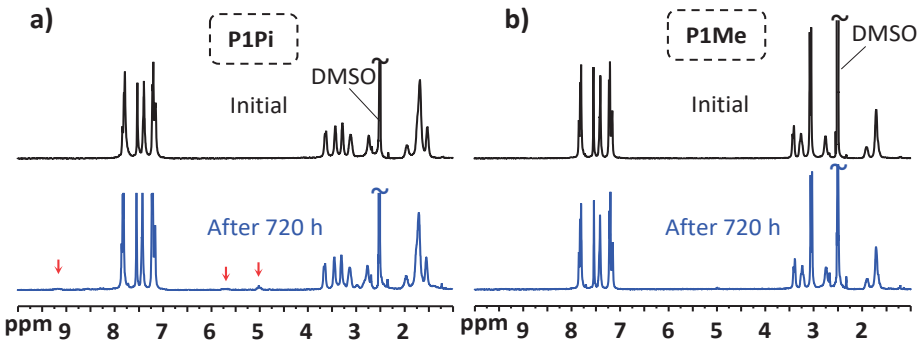

Figure 31. ^{1}H NMR spectra of **P1Pi** (a) and **P1Me** (b) recorded in DMSO-d_6/TFA before and after 720 h immersion in 2 M NaOH solutions at 90 °C (a). TFA was added to shift the water signals (originally at 3.3 ppm), revealing sample signals between 3.0 and 3.5 ppm. The red arrows point out new signals originating from degradation products.

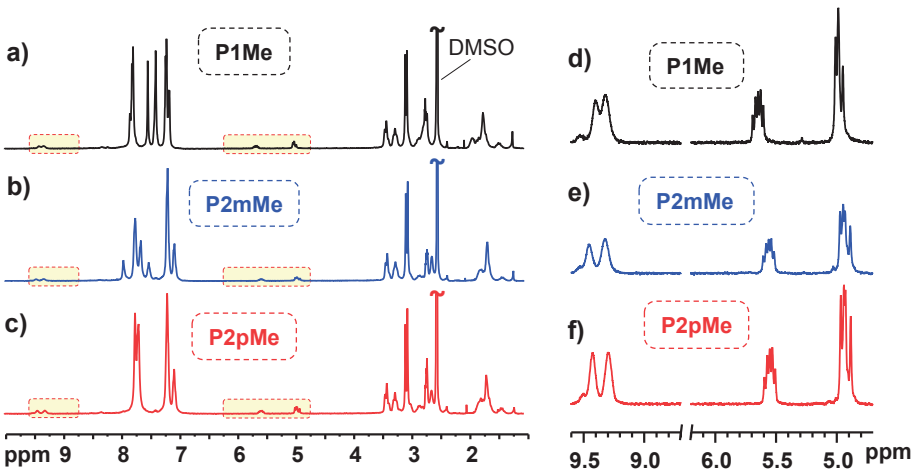

Figure 32. ^{1}H NMR spectra of **P1Me**(a), **P2Me**(b) and **P2pMe**(c) recorded in DMSO-d_6/TFA after 168 h of immersion in 2 M NaOH solutions at 120 °C (a). TFA was added to shift the water signals (originally at 3.3 ppm), revealing sample signals between 3.0 and 3.5 ppm. Expansion of the regions between 4.7–6.2 and 8.7–9.6 ppm (marked by red dashed boxes) are also shown (d,e,f).

functionalized with DMP. Under the same conditions, **P1Me**, **P2mMe** and **P2pMe** had less than 5% ionic loss (**Table 4**). Notably, the PAA-based HEMs displayed no significant change in the aromatic region (7.0-8.0 ppm) after 720 h of storage in 2 M NaOH at 90 °C, which further confirmed the excellent stability of the PAA backbone (**Figure 31**). As the total ionic loss of **P1Me**, **P2mMe** and **P2pMe** at 90°C was low and difficult to quantify, an additional study at 120 °C was performed to enable a comparison of the alkaline stability of these HEMs. After 168 h of storage at this extreme temperature, the total cationic loss of **P1Me**, **P2mMe** and **P2pMe** was 33, 27 and 35%, respectively (**Figure 32**). **P2mMe** degraded significantly less than the other HEMs, suggesting that the more flexible pendant spacer and polymer backbone had a positive impact on the alkaline stability of HEMs.

3.4. Influence of chemical structure on the alkaline stability of hydroxide exchange membranes

In order to develop alkali-stable polymers and HEMs suitable for application in FCs, it is important to study the relationship between the chemical structure and alkaline stability. The wide variation in the conditions of the alkaline stability studies hinders a direct quantitative comparison between the HEMs. However, the variation reflects the overall trend in the change of the alkaline stability. Due to the low alkaline stability of PAES-based HEMs, the conditions of the alkaline stability study in Paper I was quite mild. The concentration of hydroxide solution was kept constant at 1 M, while the temperature varied from 20 to 60 °C. In later projects, since the HEMs were more alkali-stable, harsher conditions were necessary to provide a better insight into both the degree and mechanism of the degradation of these materials. The temperature was increased to 80, 90 and 120 °C, and the hydroxide concentration was increased to 2 M. **Table 5** gives the conditions and results of alkaline stability studies of some representative HEMs in each project.

As mentioned above, the alkaline stability of HEMs is not only correlated to the alkaline stability of their cations, but also influenced by the structure of the backbones and the polymer architecture. Regarding the backbone structure, out of the three polymer backbones investigated in this thesis work (**Figure 8**), PAES gave HEMs with the lowest alkaline stability. PAES-based HEMs degraded already after 168 h of immersion in 1 M NaOH aq. solution at 40 °C. At 60 °C, the ionic loss of these membranes was estimated to be more than 40%. In addition to the degradation of the QA cations, the PAES backbones also degraded, leading to deteriorated mechanical properties. Despite having the same QA cations as **PAES-spiro-pip** (**Figure 7a**, x=2), the spiro-ionenes were significantly more stable than the PAES-based polymers. After 672 h in 1 M KOD/D_2O at 80 °C, these polymers showed no

Table 5. Conditions and results of alkaline stability studies of some representative HEMs in this thesis work.[a]

HEM	Conditions			Ionic loss (%)	Paper
	T (°C)	[OH^-] (M)	*t* (h)		
PAES-spiro-aze	40	1	168	5	I
	60	1	168	> 40	
Spiro-ionene 1[b]	80	1	672	not observed	II
	120	1	336	25	
Spiro-ionene 2[b]	80	1	1896	not observed	
	120	1	336	10	
PTPipQ8	90	2	720	73	III
PTPipQ1	90	2	720	8	
P6Ph-2.2	90	2	720	20	IV
	120	2	360	> 50	
P1Pi	90	2	720	10	V
	90	2	2900	27	
P1Me	90	2	720	<5	
	90	2	2900	13	
	120	2	168	33	
P2mMe	120	2	168	27	

[a] Alkaline stability studies of all HEMs except for the spiro-ionenes were performed in aq. NaOH solutions. ^{1}H NMR spectroscopy was used to estimate the ionic losses. [b] The alkaline stability study of spiro-ionenes was performed in 1 M KOD/D_2O solution.

detectable signs of degradation. The alkaline stability of PAA-based HEMs was comparable with that of the spiro-ionenes. Some PAA-based HEMs showed less than 5% ionic loss after storage in 2 M NaOH aq. solution at 90 °C during 720 h (**Table 5**). Moreover, no detectable degradation of the PAA backbone was observed.

Regarding the polymer architecture, the attachment of QA cations via flexible spacers (**Figure 9c**) improved the alkaline stability. For example, after 720 h of storage in 2 M NaOH aq. solution at 90 °C, **P1Me** and **P2pMe**, both with DMP cations attached to PAA backbones via spacers, had less than 5% ionic loss. Under

the same conditions, the ionic loss of **PTPipQ1**, having DMP cations directly attached to a PAA backbone, was ~ 8%. A more substantial improvement was observed when comparing HEMs functionalized with ASU. After 720 h of immersion in 2 M aq. NaOH solution at 90 °C, the total ionic loss of **P1Pi**, with the spacers, was only 10%. This was a significant decrease in comparison with the 20% ionic loss of **P6Ph-*z***, which had ASU directly attached to the polymer backbone. Not only the PAA-based HEMs, but also the spiro-ionenes benefited from the introduction of spacers. Spiro-ionene **2**, which had spacers, displayed a significantly lower degree of degradation than spiro-ionene **1**(**Table 5**).

The positive influence of the spacers was possibly due to their ability to facilitate ring-strain relaxation in the *N*-alicyclic QA cations. As previously explained (chapter 1.2.1), the alkaline stability of the *N*-alicyclic QA cations depended on the activation energy of the degradation reactions, which is the difference in energy between the transition states and the original cations. Due to the low ring-strain of 5- and 6-membered ring, the energy of free ASU and DMP cations was low. However, when these cations were incorporated into polymers, their ring relaxation might be restricted by the stiff polymer chains, leading to an increase in free energy. This would consequently result in a lower activation energy of degradation reactions and a lower alkaline stability of the cations. The attachment to a polymer chain disfavored the bulky and more rigid ASU to a greater degree than DMP. While free ASU was more stable in alkaline conditions than DMP (**Table 1**), polymers functionalized with ASU cations were less stable than their DMP-functionalized counterparts (**Table 5**). Incorporation of ASU cations via longer, more flexible spacers might help reduce the restriction imposed by the polymer backbone, thus lowering the free energy and enhancing the alkaline stability of these cations.

4. Conclusion and future outlook

The current thesis presents strategies employed and achievements accomplished in developing alkali-stable HEMs functionalized with *N*-alicyclic QA cations. By employing diverse synthetic methods, 19 HEMs with a variety of cations, backbones and polymer architectures were successfully synthesized. The characterization of these HEMs, with focus on their hydroxide conductivity, water uptake, thermal stability and thermochemical stability made it possible to establish a relationship between these properties and the chemical structure of the HEMs.

Amongst the three polymer types investigated, PAA was found to be the optimal polymer backbone for HEMs. PAES-based HEMs had the undeniable advantage of easy synthesis, high hydroxide conductivity and good mechanical properties, but they also possessed low alkaline stability, and were thus unsuitable for FC application. In contrast, the spiro-ionenes had excellent alkaline stability, but their potential for structure variation was limited, making tailoring and optimization of their properties difficult. PAA-based HEMs had the combined advantage of the aforementioned polymer types. The aryl ether-free PAA backbones were tough and alkali-resistant. The synthesis of PAA via super acid mediated polyhydroxyalkylation was highly efficient and versatile. Since the method can be applied for a wide variety of monomers, the chemical structure of the resultant polymers was easily modified to achieve desirable properties.

Regarding the choice of cations, polymers functionalized with DMP cations were more alkali-stable than counterparts functionalized with other *N*-methylalkylpiperidinium or ASU cations. This finding was in contrast with a previous study that reported on an exceptional alkaline stability of an ASU bromide salt. The close proximity to rigid polymer backbones restricting ring relaxation of the cyclic QA cations might be the reason for the decreased alkaline stability. The ring strain relaxation could be facilitated by separating the cations from the backbone through flexible spacers. The introduction of spacers had positive effects not only on the alkaline stability but also on the hydroxide conductivity as it promote phase separation as well.

Out of the 19 HEMs synthesized and investigated in this thesis work, HEM based on **P2mMe**, with DMP cations attached to a PAA backbone via flexible spacers was the most suited to be used as polymeric electrolyte for FC. **P2mMe** membrane

demonstrated a good balance between hydroxide conductivity and water uptake. At 80 °C, the membrane reached a high conductivity of 146 mS cm^{-1} while its water uptake still remained reasonable at 103%. The HEM also had a high thermal and alkaline stability. The decomposition temperature $T_{d,95}$ of **P2mMe** AEM in bromide form was 269 °C under N_2 atmosphere. The HEM displayed less than 5% ionic loss after 720 h of storage in 2 M NaOH aq. Solution at 90 °C.

Future works with these HEMs include further investigation of in-situ fuel cell performance, as well as optimization and upscaling of the polymer synthesis. The positive results obtained in this thesis work also encourage further development of HEMs based on *N*-alicyclic QA cations. A natural approach would be to continue to employ a PAA backbone, but to use longer and more flexible spacers to connect it with the cations. Even though DMP seemed a more suitable choice of cations than ASU, the introduction of more flexible spacers might change the picture. Therefore, HEMs functionalized with DMP as well as with ASU should be included in future studies.

5. Popular science summary

Climate change is ranked amongst the most serious global issues that the world is currently facing. Many scientific reports have demonstrated the connection between the more frequently occurring natural disasters during the last decade and the human-caused global warming driven by accelerating emissions of carbon dioxide. There is therefore an urgent need to reduce the emissions of atmospheric carbon dioxide by replacing fossil fuels with sustainable and environmentally friendly energy sources, including wind and solar power, biofuels and hydrogen. The utilization of these energy sources requires efficient conversion and storage. This can be achieved by the development of efficient electrochemical devices such as redox flow batteries, electrolyzers and fuel cells. Ion exchange membranes separate the electrodes and allow the transport of specific ions in these devices. They are thus crucial components that to a large degree control their performance and lifetime. Hence, membranes must be specifically developed for each application to satisfy a specific set of requirements.

Ion exchange membranes are semipermeable and promote transportation of ions and water, while preventing cross-over of fuel and oxygen gases. These membranes are divided into two main types: anion exchange membranes and proton exchange membranes (PEMs). They facilitate the transport of anions and cations, respectively. The present thesis work is dedicated to the synthesis, study and development of hydroxide exchange membranes (HEMs), a subclass of anion exchange membranes, for fuel cell application. Due to the alkaline operating conditions, fuel cells using HEMs have a crucial advantage over the commercial ones using PEMs. They do not require expensive and rare platinum-group metal catalysts and can utilize a wider range of fuels. However, the low chemical stability and the lower ion conductivity of HEMs in comparison with PEMs are significant challenges to a wider application and commercialization of HEM fuel cells.

HEMs typically consist of hydrophobic polymeric backbones tethered with cations. The backbone is responsible for the integrity and mechanical properties of the membrane. Meanwhile, the type, concentration, placement and distribution of the cations along the backbone influence the conductivity, as well as the alkaline and thermal stability of the membrane. Previous studies have demonstrated that a specific class of cations, alicyclic quaternary ammonium (QA) cations, are exceptionally stable in alkaline media. We have therefore decided to investigate these cations to

improve the alkaline stability of HEMs. However, the incorporation of alicyclic QA cations into polymer structures is a significant challenge that required new synthetic strategies.

Throughout this work, we have explored diverse synthetic strategies to incorporate alicyclic QA cations into several different polymer backbone types. The nature and placement of the cations were also varied to study the influence on the conductivity, water uptake and stability of the resulting HEMs. These are key properties that determine the performance and lifetime of HEMs in fuel cells. The membranes most suitable for use in fuel cells were those that had dimethylpiperidinium cations attached to a poly (arylene alkylene) backbone via flexible links. They presented elevated conductivity, reasonable water uptake and high stability. The results of the present study has provided new knowledge about the structure-properties relationship and has indicated directions for further improvements of HEM materials for energy applications.

6. References

1. IPCC. Summary for Policymakers. In *Climate Change 2013: The Physical Science Basis. Contribution of Working Group I to the Fifth Assessment Report of the Intergovernmental Panel on Climate Change*, Stocker, T. F.; Qin, D.; Plattner, G.-K.; Tignor, M.; Allen, S. K.; Boschung, J.; Nauels, A.; Xia, Y.; Bex, V.; Midgley, P. M., Eds. Cambridge University Press: Cambridge, United Kingdom and New York, NY, USA, 2013; pp 1–30.
2. IPCC. Summary for Policymakers. In *Global warming of 1.5°C. An IPCC Special Report on the impacts of global warming of 1.5°C above pre-industrial levels and related global greenhouse gas emission pathways, in the context of strengthening the global response to the threat of climate change, sustainable development, and efforts to eradicate poverty*, Masson-Delmotte, V.; Zhai, P.; Pörtner, H. O.; Roberts, D.; Skea, J.; P.R.Shukla; Pirani, A.; Moufouma-Okia, W.; C.Péan; Pidcock, R.; Connors, S.; Matthews, J. B. R.; Chen, Y.; Zhou, X.; Gomis, M. I.; Lonnoy, E.; Maycock, T.; Tignor, M.; Waterfield, T., Eds. In Press: 2018; pp 1–24.
3. IPCC. Summary for Policymakers. In *IPCC Special Report on Renewable Energy Sources and Climate Change Mitigation*, Edenhofer, O.; R. Pichs-Madruga; Y. Sokona; K. Seyboth; P. Matschoss; S. Kadner; T. Zwickel; P. Eickemeier; G. Hansen; S. Schlömer; Stechow, C. v., Eds. Cambridge University Press: Cambridge, United Kingdom and New York, NY, USA, 2011; pp 1–24.
4. Hannan, M. A.; Hoque, M. M.; Mohamed, A.; Ayob, A. *Renewable and Sustainable Energy Reviews* **2017**, *69*, 771-789.
5. Zakeri, B.; Syri, S. *Renew. Sust. Energ. Rev.* **2015**, *42*, 569-596.
6. Yang, Z.; Zhang, J.; Kintner-Meyer, M. C. W.; Lu, X.; Choi, D.; Lemmon, J. P.; Liu, J. *Chem. Rev.* **2011**, *111*, 3577-3613.
7. Dunn, B.; Kamath, H.; Tarascon, J.-M. *Science* **2011**, *334*, 928-935.
8. Weber, A. Z.; Mench, M. M.; Meyers, J. P.; Ross, P. N.; Gostick, J. T.; Liu, Q. *J. Appl. Electrochem.* **2011**, *41*, 1137.
9. Díaz-González, F.; Sumper, A.; Gomis-Bellmunt, O.; Villafáfila-Robles, R. *Renewable and Sustainable Energy Reviews* **2012**, *16*, 2154-2171.
10. Holladay, J. D.; Hu, J.; King, D. L.; Wang, Y. *Catal. Today* **2009**, *139*, 244-260.
11. Carmo, M.; Fritz, D. L.; Mergel, J.; Stolten, D. *Int. J. Hydrogen Energy* **2013**, *38*, 4901-4934.
12. Marini, S.; Salvi, P.; Nelli, P.; Pesenti, R.; Villa, M.; Berrettoni, M.; Zangari, G.; Kiros, Y. *Electrochim. Acta* **2012**, *82*, 384-391.

13. Zeng, K.; Zhang, D. *Prog. Energy Combust. Sci.* **2010,** *36*, 307-326.
14. Götz, M.; Lefebvre, J.; Mörs, F.; McDaniel Koch, A.; Graf, F.; Bajohr, S.; Reimert, R.; Kolb, T. *Renewable Energy* **2016,** *85*, 1371-1390.
15. Yilanci, A.; Dincer, I.; Ozturk, H. K. *Prog. Energy Combust. Sci.* **2009,** *35*, 231-244.
16. Kirubakaran, A.; Jain, S.; Nema, R. K. *Renewable and Sustainable Energy Reviews* **2009,** *13*, 2430-2440.
17. Cano, Z. P.; Banham, D.; Ye, S.; Hintennach, A.; Lu, J.; Fowler, M.; Chen, Z. *Nature Energy* **2018,** *3*, 279-289.
18. Heinzel, A.; Hebling, C.; Müller, M.; Zedda, M.; Müller, C. *J. Power Sources* **2002,** *105*, 250-255.
19. Wilberforce, T.; Alaswad, A.; Palumbo, A.; Dassisti, M.; Olabi, A. G. *Int. J. Hydrogen Energy* **2016,** *41*, 16509-16522.
20. Li, X.; Zhang, H.; Mai, Z.; Zhang, H.; Vankelecom, I. *Energy Environ. Sci.* **2011,** *4*, 1147-1160.
21. Tanaka, Y. 22 - Fuel Cell. In *Ion Exchange Membranes (Second Edition)*, Tanaka, Y., Ed. Elsevier: Amsterdam, 2015; pp 459-470.
22. Tanaka, Y. 12 - Electrodialysis. In *Ion Exchange Membranes (Second Edition)*, Tanaka, Y., Ed. Elsevier: Amsterdam, 2015; pp 255-293.
23. Tanaka, Y. 23 - Redox Flow Battery. In *Ion Exchange Membranes (Second Edition)*, Tanaka, Y., Ed. Elsevier: Amsterdam, 2015; pp 471-485.
24. Tanaka, Y. 1 - Preparation of Ion Exchange Membranes. In *Ion Exchange Membranes (Second Edition)*, Tanaka, Y., Ed. Elsevier: Amsterdam, 2015; pp 3-28.
25. Grove, W. R. *The London, Edinburgh, and Dublin Philosophical Magazine and Journal of Science* **1839,** *15*, 287-293.
26. Grove, W. R. *The London, Edinburgh, and Dublin Philosophical Magazine and Journal of Science* **1839,** *14*, 127-130.
27. Stone, C.; Morrison, A. E. *Solid State Ionics* **2002,** *152-153*, 1-13.
28. Steilen, M.; Jörissen, L. Chapter 10 - Hydrogen Conversion into Electricity and Thermal Energy by Fuel Cells: Use of H2-Systems and Batteries. In *Electrochemical Energy Storage for Renewable Sources and Grid Balancing*, Moseley, P. T.; Garche, J., Eds. Elsevier: Amsterdam, 2015; pp 143-158.
29. Cohn, E. M. NASA's Fuel Cell Program. In *Fuel Cell Systems*, AMERICAN CHEMICAL SOCIETY: 1969; Vol. 47, pp 1-8.
30. Monaghan, M. L. Chapter One - Introduction. In *Internal Combustion Engines*, Arcoumanis, C., Ed. Academic Press: 1988; pp 1-30.
31. Holmberg, K.; Andersson, P.; Erdemir, A. *Tribology International* **2012,** *47*, 221-234.
32. Chu, S.; Majumdar, A. *Nature* **2012,** *488*, 294.
33. Kunze, J.; Paschos, O.; Stimming, U. Fuel Cell Comparison to Alternate Technologies. In *Fuel Cells: Selected Entries from the Encyclopedia of Sustainability Science and Technology*, Kreuer, K.-D., Ed. Springer New York: New York, NY, 2013; pp 77-95.

34. Naber, J. D.; Johnson, J. E. 8 - Internal combustion engine cycles and concepts. In *Alternative Fuels and Advanced Vehicle Technologies for Improved Environmental Performance*, Folkson, R., Ed. Woodhead Publishing: 2014; pp 197-224.
35. Slade, R. C. T.; Kizewski, J. P.; Poynton, S. D.; Zeng, R.; Varcoe, J. R. Alkaline Membrane Fuel Cells. In *Fuel Cells: Selected Entries from the Encyclopedia of Sustainability Science and Technology*, Kreuer, K.-D., Ed. Springer New York: New York, NY, 2013; pp 9-29.
36. Scherer, G. G. Fuel Cell Types and Their Electrochemistry. In *Fuel Cells: Selected Entries from the Encyclopedia of Sustainability Science and Technology*, Kreuer, K.-D., Ed. Springer New York: New York, NY, 2013; pp 97-119.
37. Atkinson, S. *Membrane Technology* **2005,** *2005*, 6-8.
38. Kamarudin, S. K.; Achmad, F.; Daud, W. R. W. *Int. J. Hydrogen Energy* **2009,** *34*, 6902-6916.
39. Kreuer, K. D. *J. Membr. Sci.* **2001,** *185*, 29-39.
40. de Frank Bruijn, A.; Janssen, G. J. M. PEM Fuel Cell Materials: Costs, Performance and Durability. In *Fuel Cells: Selected Entries from the Encyclopedia of Sustainability Science and Technology*, Kreuer, K.-D., Ed. Springer New York: New York, NY, 2013; pp 249-303.
41. Paddison, S. J.; Gasteiger, H. A. PEM Fuel Cells, Materials and Design Development Challenges. In *Fuel Cells: Selected Entries from the Encyclopedia of Sustainability Science and Technology*, Kreuer, K.-D., Ed. Springer New York: New York, NY, 2013; pp 341-367.
42. Zhang, J. PEM Fuel Cells and Platinum-Based Electrocatalysts. In *Fuel Cells: Selected Entries from the Encyclopedia of Sustainability Science and Technology*, Kreuer, K.-D., Ed. Springer New York: New York, NY, 2013; pp 305-340.
43. Hamrock, S. J.; Herring, A. M. Proton Exchange Membrane Fuel Cells: High-Temperature, Low-Humidity Operation. In *Fuel Cells: Selected Entries from the Encyclopedia of Sustainability Science and Technology*, Kreuer, K.-D., Ed. Springer New York: New York, NY, 2013; pp 577-605.
44. Haile, S. M.; Boysen, D. A.; Chisholm, C. R. I.; Merle, R. B. *Nature* **2001,** *410*, 910-913.
45. Boysen, D. A.; Uda, T.; Chisholm, C. R. I.; Haile, S. M. *Science* **2004,** *303*, 68-70.
46. Kanuri, S. V.; Motupally, S. Phosphoric Acid Fuel Cells for Stationary Applications. In *Fuel Cells: Selected Entries from the Encyclopedia of Sustainability Science and Technology*, Kreuer, K.-D., Ed. Springer New York: New York, NY, 2013; pp 369-389.
47. Atkinson, A.; Skinner, S. J.; Kilner, J. A. Solid Oxide Fuel Cells. In *Fuel Cells: Selected Entries from the Encyclopedia of Sustainability Science and Technology*, Kreuer, K.-D., Ed. Springer New York: New York, NY, 2013; pp 657-685.
48. Yokokawa, H.; Horita, T. Solid Oxide Fuel Cell Materials: Durability, Reliability and Cost. In *Fuel Cells: Selected Entries from the Encyclopedia of Sustainability Science and Technology*, Kreuer, K.-D., Ed. Springer New York: New York, NY, 2013; pp 607-656.

49. Poynton, S. D.; Kizewski, J. P.; Slade, R. C. T.; Varcoe, J. R. *Solid State Ionics* **2010,** *181*, 219-222.
50. Li, Y. S.; Zhao, T. S.; Liang, Z. X. *J. Power Sources* **2009,** *187*, 387-392.
51. Gu, S.; Sheng, W.; Cai, R.; Alia, S. M.; Song, S.; Jensen, K. O.; Yan, Y. *Chem. Commun.* **2013,** *49*, 131-133.
52. Varcoe, J. R.; Atanassov, P.; Dekel, D. R.; Herring, A. M.; Hickner, M. A.; Kohl, P. A.; Kucernak, A. R.; Mustain, W. E.; Nijmeijer, K.; Scott, K.; Xu, T.; Zhuang, L. *Energy Environ. Sci.* **2014,** *7*, 3135-3191.
53. Fang, Y.; Yang, X.; Wang, L.; Liu, Y. *Electrochim. Acta* **2013,** *90*, 421-425.
54. Guo, J.; Hsu, A.; Chu, D.; Chen, R. *The Journal of Physical Chemistry C* **2010,** *114*, 4324-4330.
55. Olson, T. S.; Pylypenko, S.; Atanassov, P.; Asazawa, K.; Yamada, K.; Tanaka, H. *The Journal of Physical Chemistry C* **2010,** *114*, 5049-5059.
56. Wu, Q.; Jiang, L.; Tang, Q.; Liu, J.; Wang, S.; Sun, G. *Electrochim. Acta* **2013,** *91*, 314-322.
57. Chen, R.; Li, H.; Chu, D.; Wang, G. *The Journal of Physical Chemistry C* **2009,** *113*, 20689-20697.
58. Ohyama, J.; Okata, Y.; Watabe, N.; Katagiri, M.; Nakamura, A.; Arikawa, H.; Shimizu, K.-i.; Takeguchi, T.; Ueda, W.; Satsuma, A. *J. Power Sources* **2014,** *245*, 998-1004.
59. Jasinski, R. *Nature* **1964,** *201*, 1212-1213.
60. Adams, L. A.; Poynton, S. D.; Tamain, C.; Slade, R. C. T.; Varcoe, J. R. *ChemSusChem* **2008,** *1*, 79-81.
61. Hickner, M. A.; Herring, A. M.; Coughlin, E. B. *J. Polym. Sci., Part B: Polym. Phys.* **2013,** *51*, 1727-1735.
62. Cheng, J.; He, G.; Zhang, F. *Int. J. Hydrogen Energy* **2015,** *40*, 7348-7360.
63. Merle, G.; Wessling, M.; Nijmeijer, K. *J. Membr. Sci.* **2011,** *377*, 1-35.
64. Marx, D.; Chandra, A.; Tuckerman, M. E. *Chem. Rev.* **2010,** *110*, 2174-2216.
65. Marino, M. G.; Melchior, J. P.; Wohlfarth, A.; Kreuer, K. D. *J. Membr. Sci.* **2014,** *464*, 61-71.
66. Stoica, D.; Alloin, F.; Marais, S.; Langevin, D.; Chappey, C.; Judeinstein, P. *The Journal of Physical Chemistry B* **2008,** *112*, 12338-12346.
67. Varcoe, J. R. *PCCP* **2007,** *9*, 1479-1486.
68. Mauritz, K. A.; Moore, R. B. *Chem. Rev.* **2004,** *104*, 4535-4586.
69. Hsu, W. Y.; Gierke, T. D. *J. Membr. Sci.* **1983,** *13*, 307-326.
70. Diat, O.; Gebel, G. *Nature Materials* **2008,** *7*, 13.
71. Li, N.; Guiver, M. D. *Macromolecules* **2014,** *47*, 2175-2198.
72. Li, N.; Wang, C.; Lee, S. Y.; Park, C. H.; Lee, Y. M.; Guiver, M. D. *Angew. Chem. Int. Ed.* **2011,** *50*, 9158-9161.
73. Peckham, T. J.; Holdcroft, S. *Adv. Mater.* **2010,** *22*, 4667-4690.
74. Vandiver, M. A.; Caire, B. R.; Carver, J. R.; Waldrop, K.; Hibbs, M. R.; Varcoe, J. R.; Herring, A. M.; Liberatore, M. W. *J. Electrochem. Soc.* **2014,** *161*, H677-H683.

75. Dang, H.-S.; Jannasch, P. *Journal of Materials Chemistry A* **2016,** *4*, 11924-11938.
76. Zhu, L.; Pan, J.; Christensen, C. M.; Lin, B.; Hickner, M. A. *Macromolecules* **2016,** *49*, 3300-3309.
77. Dang, H. S.; Weiber, E. A.; Jannasch, P. *Journal of Materials Chemistry A* **2015,** *3*, 5280-5284.
78. Lee, W.-H.; Mohanty, A. D.; Bae, C. *ACS Macro Letters* **2015,** *4*, 453-457.
79. Lee, W.-H.; Kim, Y. S.; Bae, C. *ACS Macro Letters* **2015,** *4*, 814-818.
80. Zhuo, Y. Z.; Lai, A. L.; Zhang, Q. G.; Zhu, A. M.; Ye, M. L.; Liu, Q. L. *Journal of Materials Chemistry A* **2015,** *3*, 18105-18114.
81. Yang, Z.; Guo, R.; Malpass-Evans, R.; Carta, M.; McKeown, N. B.; Guiver, M. D.; Wu, L.; Xu, T. *Angew. Chem. Int. Ed.* **2016,** *55*, 11499-11502.
82. Li, N.; Wang, L.; Hickner, M. *Chem. Commun.* **2014,** *50*, 4092-4095.
83. Ponce-González, J.; Whelligan, D. K.; Wang, L.; Bance-Soualhi, R.; Wang, Y.; Peng, Y.; Peng, H.; Apperley, D. C.; Sarode, H. N.; Pandey, T. P.; Divekar, A. G.; Seifert, S.; Herring, A. M.; Zhuang, L.; Varcoe, J. R. *Energy Environ. Sci.* **2016,** *9*, 3724-3735.
84. Olsson, J. S.; Pham, T. H.; Jannasch, P. *Adv. Funct. Mater.* **2018,** *28*, 1702758.
85. Dekel, D. R. *J. Power Sources* **2018,** *375*, 158-169.
86. Lee, K. H.; Cho, D. H.; Kim, Y. M.; Moon, S. J.; Seong, J. G.; Shin, D. W.; Sohn, J.-Y.; Kim, J. F.; Lee, Y. M. *Energy Environ. Sci.* **2017,** *10*, 275-285.
87. Edson, J. B.; Macomber, C. S.; Pivovar, B. S.; Boncella, J. M. *J. Membr. Sci.* **2012,** *399–400*, 49-59.
88. Chempath, S.; Einsla, B. R.; Pratt, L. R.; Macomber, C. S.; Boncella, J. M.; Rau, J. A.; Pivovar, B. S. *Journal of Physical Chemistry C* **2008,** *112*, 3179-3182.
89. Cerichelli, G.; Illuminati, G.; Lillocci, C. *The Journal of Organic Chemistry* **1980,** *45*, 3952-3957.
90. Cope, A. C.; Mehta, A. S. *J. Am. Chem. Soc.* **1963,** *85*, 1949-1952.
91. Marino, M. G.; Kreuer, K. D. *ChemSusChem* **2015,** *8*, 513-523.
92. Chempath, S.; Boncella, J. M.; Pratt, L. R.; Henson, N.; Pivovar, B. S. *The Journal of Physical Chemistry C* **2010,** *114*, 11977-11983.
93. Archer, D. A. *Journal of the Chemical Society C: Organic* **1971**, 1329-1331.
94. Kantor, S. W.; Hauser, C. R. *J. Am. Chem. Soc.* **1951,** *73*, 4122-4131.
95. Arges, C. G.; Ramani, V. *Proc. Natl. Acad. Sci. U. S. A.* **2013,** *110*, 2490-2495.
96. Mohanty, A. D.; Tignor, S. E.; Krause, J. A.; Choe, Y. K.; Bae, C. *Macromolecules* **2016,** *49*, 3361-3372.
97. Choe, Y.-K.; Fujimoto, C.; Lee, K.-S.; Dalton, L. T.; Ayers, K.; Henson, N. J.; Kim, Y. S. *Chem. Mater.* **2014,** *26*, 5675-5682.
98. Fujimoto, C.; Kim, D.-S.; Hibbs, M.; Wrobleski, D.; Kim, Y. S. *J. Membr. Sci.* **2012,** *423-424*, 438-449.
99. Amel, A.; Zhu, L.; Hickner, M.; Ein-Eli, Y. *J. Electrochem. Soc.* **2014,** *161*, F615-F621.

100. Miyanishi, S.; Yamaguchi, T. *PCCP* **2016,** *18*, 12009-12023.
101. Hibbs, M. R. *J. Polym. Sci., Part B: Polym. Phys.* **2013,** *51*, 1736-1742.
102. Janarthanan, R.; Pilli, S. K.; Horan, J. L.; Gamarra, D. A.; Hibbs, M. R.; Herring, A. M. *J. Electrochem. Soc.* **2014,** *161*, F944-F950.
103. Wang, J.; Zhao, Y.; Setzler, B. P.; Rojas-Carbonell, S.; Ben Yehuda, C.; Amel, A.; Page, M.; Wang, L.; Hu, K.; Shi, L.; Gottesfeld, S.; Xu, B.; Yan, Y. *Nature Energy* **2019,** *4*, 392-398.
104. Miyake, J.; Taki, R.; Mochizuki, T.; Shimizu, R.; Akiyama, R.; Uchida, M.; Miyatake, K. *Sci. Adv.* **2017,** *3*, eaao0476.
105. Pham, T. H.; Olsson, J. S.; Jannasch, P. *J. Mater. Chem. A* **2019,** *7*, 15895-15906.
106. Nunez, S. A.; Hickner, M. A. *Acs Macro Letters* **2013,** *2*, 49-52.
107. Pham, T. H.; Jannasch, P. *ACS Macro Letters* **2015,** *4*, 1370-1375.
108. Thomas, O. D.; Soo, K. J.; Peckham, T. J.; Kulkarni, M. P.; Holdcroft, S. *J. Am. Chem. Soc.* **2012,** *134*, 10753-6.
109. Hugar, K. M.; Kostalik, H. A.; Coates, G. W. *J. Am. Chem. Soc.* **2015,** *137*, 8730-8737.
110. Mohanty, A. D.; Bae, C. *Journal of Materials Chemistry A* **2014,** *2*, 17314-17320.
111. Dang, H.-S.; Jannasch, P. *Journal of Materials Chemistry A* **2017,** *5*, 21965-21978.
112. Hahn, S.-J.; Won, M.; Kim, T.-H. *Polym. Bull.* **2013,** *70*, 3373-3385.
113. Morandi, C. G.; Peach, R.; Krieg, H. M.; Kerres, J. *Journal of Materials Chemistry A* **2015,** *3*, 1110-1120.
114. Yang, Z.; Zhou, J.; Wang, S.; Hou, J.; Wu, L.; Xu, T. *Journal of Materials Chemistry A* **2015,** *3*, 15015-15019.
115. Liu, Y.; Zhang, B.; Kinsinger, C. L.; Yang, Y.; Seifert, S.; Yan, Y.; Mark Maupin, C.; Liberatore, M. W.; Herring, A. M. *J. Membr. Sci.* **2016,** *506*, 50-59.
116. Wang, J.; Li, S.; Zhang, S. *Macromolecules* **2010,** *43*, 3890-3896.
117. Qu, C.; Zhang, H.; Zhang, F.; Liu, B. *J. Mater. Chem.* **2012,** *22*, 8203-8207.
118. Liu, L.; Li, Q.; Dai, J.; Wang, H.; Jin, B.; Bai, R. *J. Membr. Sci.* **2014,** *453*, 52-60.
119. Miyake, J.; Fukasawa, K.; Watanabe, M.; Miyatake, K. *J. Polym. Sci., Part A: Polym. Chem.* **2014,** *52*, 383-389.
120. Li, Y.; Xu, T.; Gong, M. *J. Membr. Sci.* **2006,** *279*, 200-208.
121. Zhang, Z.; Wu, L.; Varcoe, J.; Li, C.; Ong, A. L.; Poynton, S.; Xu, T. *Journal of Materials Chemistry A* **2013,** *1*, 2595-2601.
122. Tomoi, M.; Yamaguchi, K.; Ando, R.; Kantake, Y.; Aosaki, Y.; Kubota, H. *J. Appl. Polym. Sci.* **1997,** *64*, 1161-1167.
123. Fan, J.; Wright, A. G.; Britton, B.; Weissbach, T.; Skalski, T. J. G.; Ward, J.; Peckham, T. J.; Holdcroft, S. *ACS Macro Letters* **2017,** *6*, 1089-1093.
124. Wright, A. G.; Weissbach, T.; Holdcroft, S. *Angew. Chem. Int. Ed.* **2016,** *55*, 4818-4821.

125. Fan, J.; Willdorf-Cohen, S.; Schibli, E. M.; Paula, Z.; Li, W.; Skalski, T. J. G.; Sergeenko, A. T.; Hohenadel, A.; Frisken, B. J.; Magliocca, E.; Mustain, W. E.; Diesendruck, C. E.; Dekel, D. R.; Holdcroft, S. *Nature Communications* **2019,** *10*, 2306.
126. Ran, J.; Wu, L.; Varcoe, J. R.; Ong, A. L.; Poynton, S. D.; Xu, T. *J. Membr. Sci.* **2012,** *415-416*, 242-249.
127. Zschocke, P.; Quellmalz, D. *J. Membr. Sci.* **1985,** *22*, 325-332.
128. Cotter, R. J. *Engineering Plastics: A Handbook of Polyarylethers*. Gordon and Breach: 1995.
129. Teoh, S. H.; Tang, Z. G.; Hastings, G. W. Thermoplastic Polymers In Biomedical Applications: Structures, Properties and Processing. In *Handbook of Biomaterial Properties*, Black, J.; Hastings, G., Eds. Springer US: Boston, MA, 1998; pp 270-301.
130. Ioan, S. *Functionalized Polysulfones: Synthesis, Characterization, and Applications*. CRC Press: 2015.
131. Meier-Haack, J.; Taeger, A.; Vogel, C.; Schlenstedt, K.; Lenk, W.; Lehmann, D. *Sep. Purif. Technol.* **2005,** *41*, 207-220.
132. Harrison, W. L.; Hickner, M. A.; Kim, Y. S.; McGrath, J. E. *Fuel Cells* **2005,** *5*, 201-212.
133. Maier, G.; Meier-Haack, J. Sulfonated Aromatic Polymers for Fuel Cell Membranes. In *Fuel Cells II*, Scherer, G. G., Ed. Springer Berlin Heidelberg: Berlin, Heidelberg, 2008; pp 1-62.
134. Borup, R.; Meyers, J.; Pivovar, B.; Kim, Y. S.; Mukundan, R.; Garland, N.; Myers, D.; Wilson, M.; Garzon, F.; Wood, D.; Zelenay, P.; More, K.; Stroh, K.; Zawodzinski, T.; Boncella, J.; McGrath, J. E.; Inaba, M.; Miyatake, K.; Hori, M.; Ota, K.; Ogumi, Z.; Miyata, S.; Nishikata, A.; Siroma, Z.; Uchimoto, Y.; Yasuda, K.; Kimijima, K.-i.; Iwashita, N. *Chem. Rev.* **2007,** *107*, 3904-3951.
135. Parker, D.; Bussink, J.; Grampel, H. T. v. d.; Wheatley, G. W.; Dorf, E. U.; Ostlinning, E.; Reinking, K.; Schubert, F.; Jünger, O. Polymers, High-Temperature. In *Ullmann's Encyclopedia of Industrial Chemistry*.
136. Rose, J. B. *Polymer* **1974,** *15*, 456-465.
137. Maiti, S.; Mandal, B. K. *Prog. Polym. Sci.* **1986,** *12*, 111-153.
138. Müllen, K.; Lex, J.; Schulz, R. C.; Walter, F. *Polym. Bull.* **1990,** *24*, 263-269.
139. Dianin, A. P. *Russian Journal of Physical Chemistry* **1891,** *23*, 488,523 and 601.
140. Olvera, L. I.; Guzmán-Gutiérrez, M. T.; Zolotukhin, M. G.; Fomine, S.; Cárdenas, J.; Ruiz-Trevino, F. A.; Villers, D.; Ezquerra, T. A.; Prokhorov, E. *Macromolecules* **2013,** *46*, 7245-7256.
141. Cruz, A. R.; Zolotukhin, M. G.; Morales, S. L.; Cardenas, J.; Cedillo, G.; Fomine, S.; Salmon, M.; Carreón-Castro, M. P. *Chem. Commun.* **2009**, 4408-4410.
142. Diaz, A. M.; Zolotukhin, M. G.; Fomine, S.; Salcedo, R.; Manero, O.; Cedillo, G.; Velasco, V. M.; Guzman, M. T.; Fritsch, D.; Khalizov, A. F. *Macromol. Rapid Commun.* **2007,** *28*, 183-187.

143. Hernández-Cruz, O.; Zolotukhin, M. G.; Fomine, S.; Alexandrova, L.; Aguilar-Lugo, C.; Ruiz-Treviño, F. A.; Ramos-Ortíz, G.; Maldonado, J. L.; Cadenas-Pliego, G. *Macromolecules* **2015,** *48*, 1026-1037.
144. Guzmán-Gutiérrez, M. T.; Nieto, D. R.; Fomine, S.; Morales, S. L.; Zolotukhin, M. G.; Hernandez, M. C. G.; Kricheldorf, H.; Wilks, E. S. *Macromolecules* **2011,** *44*, 194-202.
145. Guzmán-Gutiérrez, M. T.; Nieto, D. R.; Fomine, S.; Morales, S. L.; Zolotukhin, M. G.; Hernandez, M. C. G.; Kricheldorf, H.; Wilks, E. S. *Macromolecules* **2011,** *44*, 194-202.
146. Menschutkin, N. Beiträge zur Kenntnis der Affinitätskoeffizienten der Alkylhaloide und der organischen Amine. In *Zeitschrift für Physikalische Chemie*, 1890; Vol. 5U, p 589.
147. Incremona, J. H.; Martin, J. C. *J. Am. Chem. Soc.* **1970,** *92*, 627-634.
148. Djerassi, C. *Chem. Rev.* **1948,** *43*, 271-317.
149. Wohl, A. *Berichte der deutschen chemischen Gesellschaft (A and B Series)* **1919,** *52*, 51-63.
150. Ziegler, K.; Schenck, G.; Krockow, E. W.; Siebert, A.; Wenz, A.; Weber, H. *Justus Liebigs Ann. Chem.* **1942,** *551*, 1-79.
151. Clayden, J.; Greeves, N.; Warren, S. *Organic Chemistry*. OUP Oxford: 2012.
152. Blanksby, S. J.; Ellison, G. B. *Acc. Chem. Res.* **2003,** *36*, 255-263.
153. Vice, S.; Bara, T.; Bauer, A.; Evans, C. A.; Ford, J.; Josien, H.; McCombie, S.; Miller, M.; Nazareno, D.; Palani, A.; Tagat, J. *The Journal of Organic Chemistry* **2001,** *66*, 2487-2492.
154. Su, J.; Wang, Y.; Lin, J.; Liang, J.; Sun, J.; Zou, X. *Dalton Transactions* **2013,** *42*, 1360-1363.
155. Cowie, J. M. G.; Arrighi, V. *Polymers: Chemistry and Physics of Modern Materials, Third Edition*. CRC Press: 2007.
156. ASTM D2857-16, "Standard Practice for Dilute Solution Viscosity of Polymers". ASTM International: West Conshohocken, PA, 2016.
157. Gebel, G.; Diat, O. *Fuel Cells* **2005,** *5*, 261-276.
158. Longworth, R.; Vaughan, D. J. *Nature* **1968,** *218*, 85-87.
159. Pauw, B. R. *J. Phys.: Condens. Matter* **2014,** *26*, 239501.
160. Williams, C. E. Structure of Ionomers : Use and Abuse of Saxs. In *Structure and Properties of Ionomers*, Pineri, M.; Eisenberg, A., Eds. Springer Netherlands: Dordrecht, 1987; pp 163-170.
161. Yarusso, D. J.; Cooper, S. L. *Macromolecules* **1983,** *16*, 1871-1880.
162. Weiber, E. A.; Jannasch, P. *J. Membr. Sci.* **2015,** *481*, 164-171.
163. Weiber, E. A.; Jannasch, P. *ChemSusChem* **2014,** *7*, 2621-2630.
164. Weiber, E. A.; Meis, D.; Jannasch, P. *Polymer Chemistry* **2015,** *6*, 1986-1996.
165. Olsson, J. S.; Pham, T. H.; Jannasch, P. *J. Membr. Sci.* **2019,** *578*, 183-195.
166. Pham, T. H.; Olsson, J. S.; Jannasch, P. *J. Am. Chem. Soc.* **2017,** *139*, 2888-2891.

7. Acknowledgements

This thesis has been performed at the Centre for Analysis and Synthesis at Lund University. It would not have been possible without all the help and support from many people, to whom I would like to give warm thanks to.

First and foremost, I would like to thank my supervisor Patric Jannasch, for giving me the wonderful opportunity to carry out my PhD study here. You have provided me inspiration, guidance and support, while still giving me the freedom to explore and try my own ideas. Thank you for trusting me even when I did not trust me myself. I cannot express how much your encouragement means to me.

I would also like to thank my co-supervisors, Frans and Bao, for your valuable advices.

I have also received tremendous help from other members of the polymer group: Annika, Son, Joel, Hannes, Christopher, Narae, Andrit, Dong, Olivier, Nitin, Monica, Matilda, Niklas, Denis, Carlos, Ping, Xiaoya, Dang and Smita. Special thanks to Annika and Son, for teaching me methods of polymerization and characterization. Joel, thank you for the wonderful collaboration. I have learnt a lot from the numerous discussions with you. Christopher, thank you for your invaluable help and advice on NMR and EIS. And Hannes, your attention to details have saved me from making awkward mistakes many times.

I would like to extend my gratitude to other colleagues at Polymat. I consider myself extremely lucky to have been part of such a wonderful division, where everyone is so friendly, positive and supportive to each other. You all have made my time as a PhD student here much more enjoyable. I will never forget all the happy lunches, coffee breaks I have had with you. And a special thanks to Laura and Christopher, for organizing and hosting the wonderful after-work activities for everyone.

I am deeply grateful to my colleagues at the Centre for Analysis and Synthesis, who have directly or indirectly helped me during my PhD. I would especially like to thank Maria, Bodil and Katarina, for your amazing assistance with administration and chemicals all these years. Also, Karl-Erik and Göran, for your help with NMR.

I would like to thank the Swedish Energy Agency, the Swedish Research Council, the Swedish Foundation for Strategic Research and the Royal Physiographic Society of Lund for the financial support.

Last but not least, I owe a huge thanks to my family for all their help and support throughout this challenging work.

Printed by Media-Tryck, Lund 2019 NORDIC SWAN ECOLABEL 3041 0903

LUND UNIVERSITY

ISBN: 978-91-7422-687-4

Centre for Analysis and Synthesis
Department of Chemistry
Faculty of Engineering
Lund University